# Blocking peripheral drive from colorectal afferents by sub-kilohertz DRG stimulation

**Longtu Chen[1], Tiantian Guo[1], Shaopeng Zhang[1], Phillip P. Smith[2], Bin Feng[1]**

[1]Department of Biomedical Engineering, University of Connecticut, Storrs, CT 06269

[2]School of Medicine, University of Connecticut Health Center, Farmington, CT 06030

Number of text pages of entire manuscript:

Number of figures: 10

Number of tables: 0

Correspondence:

Bin Feng, Ph.D.

Department of Biomedical Engineering

University of Connecticut

260 Glenbrook Road, Unit 3247

Storrs, CT 06269-3247, USA

E-mail: fengb@uconn.edu

Phone: 860-486-6435, fax: 860-486-2500

Lab URL: https://npr.bme.uconn.edu

**Abstract**

Clinical evidence indicates dorsal root ganglion (DRG) stimulation effectively reduces pain without the need to evoke paresthesia. This paresthesia-free anesthesia by DRG stimulation can be promising to treat pain from the viscera, where paresthesia usually cannot be produced. Here, we explored the mechanisms and parameters for DRG stimulation using an *ex vivo* preparation with mouse distal colon and rectum (colorectum), pelvic nerve, L6 DRG, and dorsal root in continuity. We conducted single-fiber recordings from split dorsal root and assessed the effect of DRG stimulation on afferent neural transmission. We determined the optimal stimulus pulse width by measuring the chronaxies of DRG stimulation to be below 216 μsec, indicating spike initiation likely at attached axons rather than somata. Sub-kilohertz DRG stimulation significantly attenuates colorectal afferent transmission (10, 50, 100, 500 and 1000 Hz), of which 50 and 100 Hz show superior blocking effects. Synchronized spinal nerve and DRG stimulation reveals a progressive increase in conduction delay by DRG stimulation, suggesting activity-dependent slowing in blocked fibers. Afferents blocked by DRG stimulation show a greater increase in conduction delay than unblocked counterparts. Mid-range frequencies (50–500 Hz) are more efficient at blocking transmission than lower or higher frequencies. In addition, DRG stimulation at 50 and 100 Hz significantly attenuates *in vivo* visceromotor responses to noxious colorectal balloon distension. This reversible conduction block in C- and Aδ-type afferents by sub-kilohertz DRG stimulation likely underlies the paresthesia-free anesthesia by DRG stimulation, thereby offering a promising new approach for managing chronic visceral pain.

## Introduction

Visceral pain is the main complaint of patients with irritable bowel syndrome (IBS) [18]. Despite recent advancement on peripherally-restricted drugs, pharmacological management of visceral pain in IBS remains challenging [9]. Neuromodulation, as a non-drug alternative, has been reported to effectively manage some chronic pain, e.g., spinal cord stimulation (SCS) and peripheral nerve stimulation (PNS) in the treatment of low back pain, neuropathic pain, and complex regional pain syndrome. In contrast, implementing neuromodulation to manage visceral pain is rarely reported. Only a handful of reports use SCS to treat visceral pain [3; 29; 30]. This discrepancy likely reflects the differential sensory innervations of visceral and non-visceral organs [17]. In non-visceral applications, SCS and PNS may suppress pain by activating large-diameter A-fibers, evoking a non-painful tingling sensation (i.e., paresthesia) that masks the sensation of pain [40; 56]. In the above reports of using SCS to treat visceral pain, no paresthesia was reported from stimulation of neurons projecting to the visceral organs. Hence, conventional neuromodulation approach of overlapping the paresthesia area with the region of pain may not be applicable to managing visceral pain.

Besides SCS and PNS, dorsal root ganglion (DRG) stimulation has emerged as a novel pain-managing approach, approved by the FDA to treat complex regional pain syndrome and peripheral causalgia in the groin and lower limbs. Recently, DRG stimulation has been reported in preclinical studies to be effective to alleviate pain related to osteoarthritis and rheumatoid arthritis in rats [39; 55]. DRG stimulation does not require paresthesia to alleviate pain, and paresthesia-free subjects obtain similar or better outcomes of pain relief [36; 53]. These clinical observations indicate that the anti-nociceptive effect of DRG stimulation is not exclusively through activating large-diameter A-fibers, but may also be contributed to by direct blockade of afferent neural

transmission as indicated by a recent report [6]. Direct evidence of blocking visceral afferent neural transmission by DRG stimulation is limited in the literature, and parameters of DRG stimulation have yet to be systematically tested and optimized. Electrophysiological studies have been conducted on dissociated DRG neurons, which differ greatly from afferents with intact DRG in their neural excitabilities [21; 27]. Using intact DRG, the effect of DRG stimulation was assessed by intracellular recordings [27; 31], which will not allow direct assessment of the through-conduction in afferent axons that can by-pass the soma.

To test the hypothesis of transmission block in visceral afferents by DRG stimulation, we developed an *ex vivo* preparation in which mouse colorectum, pelvic nerve, L6 DRG, and dorsal root were harvested in continuity. We conducted experiments with tissues harvested from mice receiving intracolonic treatment of 2,4,6-trinitrobenzenesulfonic acid (TNBS), a model of post-infectious irritable bowel syndrome [20]. We focused on exploring the blocking effect of sub-kilohertz DRG stimulation in both C-fibers and Aδ-fibers, which make up the vast majority of colorectal afferents [19]. We first identified the chronaxie of DRG stimulation by measuring the strength-duration curves and set the stimulus pulse width close to the chronaxie for optimal energy efficiency of DRG stimulation. We then systematically investigated the blocking effect of DRG stimulation by conducting single-fiber recordings from split L6 dorsal roots of action potentials evoked from peripheral endings in the colorectum. Also, we developed a synchronized protocol to electrically evoke action potentials while delivering DRG stimulation, revealing an instantaneous and progressive increase in conduction delay by DRG stimulation. To confirm the functional relevance of our *ex-vivo* findings, we verified that sub-kilohertz DRG stimulation was effective in suppressing visceral pain by measuring *in vivo* visceromotor responses to noxious colorectal balloon distension. Portions of the data have been reported previously in abstract form [7; 8].

## Methods

All experimental procedures were approved by the University of Connecticut Institutional Animal Care and Use Committee. All the mice used in the following experiments were housed in pathogen free facilities which are PHS assured and AAALAC accredited following the Guide for the Care and Use of Laboratory Animals Eighth Edition. Mice resided in individual ventilated caging systems in polycarbonate cages (Animal Care System M.I.C.E.) and were provided with contact bedding (Envigo T7990 B.G. Irradiated Teklad Sani Chips). Mice were fed ad lib with either 2918 Irradiated Teklad Global 18% Rodent Diet or 7904 Irradiated S2335 Mouse Breeder Diet supplied by Envigo and supplied with reverse osmosis water chlorinated to 2 ppm using a water bottle. Nestlets and huts were supplied for enrichment. Rodent housing temperature was set for 73.5 F with a range from 70–77 F. Humidity was set for 50% with a range of 35–65%. Mice were housed with a max of 5 animals per cage. All animals were housed on a 12:12 light: dark cycle. Animals were observed daily by the ACS staff. Cages were changed every two weeks.

### Intracolonic TNBS treatment

Detailed treatment procedures were reported previously [20]. Briefly, mice were anesthetized by isoflurane inhalation, transanally administered with TNBS (0.2 ml @ 10 mg/ml in 50% ethanol; Sigma-Aldrich, St. Louis, MO) via a 22-gauge feeding needle (#18061-22, Fine Science Tools, Foster City, CA), and held in a head down position (~30°) for five minutes to preserve TNBS in the colorectum. Dietary gel (NGB-1, Bio-Serv, Flemington, NJ) was provided to mice showing severe weight loss (> 5% original body weight). Mice at 7–14 days following TNBS treatment were used in current study, a time span of colorectal hypersensitivity as systematically characterized by our prior study [20].

**Characterization of the strength-duration curve of DRG stimulation**

To achieve efficient electrical stimulation, it is necessary to deliver a stimulus with pulse width close to the chronaxie of the strength-duration curve, at which excitable tissues are activated by the least amount of electrical energy [22]. Here, we determined the strength-duration curve of mouse DRG stimulation by measuring the threshold stimulus amplitude at different stimulus pulse widths from 20 μsec to 2 msec. To accurately assess the stimulus threshold, the evoked DRG responses were recorded using two independent methods: single-fiber recordings at the attached dorsal roots from C57BL/6 mice, and optical recordings of intracellular $Ca^{2+}$ transients in DRG somata from a transgenic mouse strain expressing GCaMP6f in sensory neurons driven by the VGLUT2 promotor [25].

*Single-fiber recordings of evoked action potentials.* C57BL/6 mice of both sexes (8–16 weeks, 25–35 g, N=10) were anesthetized by 2% isoflurane inhalation followed by intraperitoneal and intramuscular injection of a ketamine/xylazine cocktail (100/10 mg per kg weight), and then euthanized by exsanguination from the right atrium and transcardiac perfusion from the left ventricle with oxygenated (95% $O_2$, 5% $CO_2$) ice-cold Krebs solution containing (mM): 117.9 NaCl, 4.7 KCl, 25 $NaHCO_3$, 1.3 $NaH_2PO_4$, 1.2 $MgSO_4$, 2.5 $CaCl_2$, and 11.1 D-glucose. Dorsal pediculectomy was performed to expose the spinal cord and DRG from T12 to S1 segments. Exsanguinated mouse carcass was then placed in a dissection chamber circulated with oxygenated ice-cold Krebs solution. The L6 DRG with attached dorsal root and a segment of the spinal nerve was carefully harvested in continuity and transferred to a custom-built recording chamber consisting of a tissue chamber and an adjacent recording chamber. The L6 DRG was placed in the tissue chamber perfused with oxygenated Krebs solution at 30°C and the dorsal root was gently pulled into the recording chamber filled with mineral oil (Fisher Scientific, East Greenwich, RI)

to enhance the signal-to-noise ratio (SNR) of the recording. The L6 dorsal root was carefully split into fine filaments (~10 μm) to achieve single-fiber recordings from individual afferent axons as shown in **Figure 1A** following a previously reported protocol [10].

*Optical GCaMP6f recordings of evoked action potentials.* Ai95 mice (C57BL/6 background) possessing homozygous GCaMP6f (strain# 28865, Jackson Laboratory, CT) were cross bred with mice carrying homozygous VGLUT2-Cre (strain# 28863, Jackson Laboratory, CT) to express GCaMP6f in glutamatergic neurons expressing type 2 vesicular glutamate transporter (VGLUT2), which is extensively present in sensory neurons innervating the colorectum [25]. Naïve (N=7) and TNBS treated (N=8) transgenic mice of both sexes (8–16 weeks, 25–35 g) with heterozygous GCaMP6f and VGLUT2-Cre genes (i.e., VGLUT2/GCaMP6f) were used for optical electrophysiological recordings. The L6 DRG was harvested following the same procedure for single-fiber recordings described above. To conduct optical GCaMP6f recordings, we used an up-right fluorescent microscope (BX51WI, Olympus, Waltham, MA) coupled with a water immersion 10x objective (UMPLFLN 10XW, 0.3 NA), which allowed visualization of the whole L6 DRG with sufficient resolution to detect $Ca^{2+}$ transients in individual DRG somata. We illuminated the DRG with a halogen epi-illumination light source and video recorded the evoked GCaMPf6 transients at 1920x1080 pixel resolution (2x2 bins) and 60–100 frames per sec using a high-speed ultra-low noise sCMOS camera (Xyla-4.2P, 82% quantum efficiency, Andor Technology, South Windsor, CT). Displayed in **Figure 1B** is a representative image frame of recorded GCaMP6f transients. The DRG diameters were measured post-hoc on captured images in ImageJ (NIH, Bethesda, MD). The actual size was derived by converting the pixel size to microns (2 μm/pixel).

*DRG stimulation protocols to characterize the strength-duration curve.* To electrically stimulate the DRG, we used a blunt-tipped needle electrode (FHC, platinum-iridium, tip size Φ

~25 μm) placed in contact with but not penetrating the capsule of the L6 DRG (i.e., the continuation of the dura mater enclosing the spinal cord) to deliver constant current stimulation (701C stimulating module, Aurora Scientific Inc., Canada). Charge-balanced bipolar stimuli (constant current, cathodic first) were delivered at 0.5 Hz with a wide range of pulse widths (PW in msec, 0.02, 0.04, 0.08, 0.1, 0.2, 0.4, 0.6, 0.8, 1, 2). The evoked action potentials were recorded either by single-fiber recordings from attached L6 dorsal root [10] or by optical GCaMP6f recordings from the DRG somata [25]. To determine the stimulus threshold, the current amplitude was fine adjusted at 0.1 mA resolution so that a pulse train containing 10 stimulus pulses evoked 3–5 action potentials.

*Determination of chronaxie.* The conduction velocity (CV) determined from single-fiber recordings serves as a criterion to classify DRG neurons into Aδ- and C-types. Aδ-type DRG neurons have CVs between 1 and 7.5 m/s and C-type less than 1 m/s [10]. Single-fiber recordings from split L6 nerve roots were filtered (bandpass filter, 300–3000 Hz), digitized at 24 kHz, and stored using the recording module of the TDT system (PZ5-32, RZ5D, Tucker-Davis Technologies [TDT], Alachua, FL). Single-fiber data were processed off-line using customized MATLAB programs (MathWorks R2019a). We set the detection threshold of action potentials as four times the root mean square (RMS) value of the 5-msec-long noise recorded right before stimulation. Conduction delay was measured between the onsets of stimulus artifacts and the evoked action potentials. CV was computed by dividing the distance between the stimulating and recording electrodes with the conduction delay. For GCaMP6f recordings, DRG neurons were grouped by soma size into small- and medium-diameter groups ($\Phi < 20$ μm, 20 μm $< \Phi <$ 35 μm), which generally correlate with C- and Aδ-type DRG neurons [44].

The threshold amplitudes of stimulus currents (I) were plotted against stimulus pulse width (d) to generate the strength-duration curve for both Aδ- and C-type DRG neurons, which were fitted by a hyperbolic function in Eq. 1 [22]:

$$I = b(1 + c/d) \quad (1)$$

where the constants b and c are the rheobase and chronaxie, respectively. Data were presented as means ± SE. Student's t-tests were performed as appropriate using SigmaPlot v9.0 (Systat Software, San Jose, CA). Differences were considered significant when $p < 0.05$.

**Effect of DRG stimulation on mouse L6 spinal afferent neural transmission**

The effect of DRG stimulation on colorectal afferent neural transmission was systematically studied in both naïve and TNBS-treated mice using a novel *ex vivo* preparation in which colorectum, pelvic nerve (PN), L6 spinal nerve, L6 DRG and L6 dorsal root (DR) were harvested in continuity, i.e., an intact colorectum-PN-DRG-DR preparation. Colorectal afferents were activated by colorectal distension (CRD) and evoked action potentials were recorded from split L6 DR by single-fiber recordings. In another series of experiments, the L6 spinal nerve (SN), DRG and DR, i.e., the SN-DRG-DR pathway was preserved to assess the instantaneous change of afferent neural transmission following each stimulus pulse train delivered to L6 DRG, allowing synchronization among action potential generation at SN, DRG stimulation, and single-fiber recording at DR. In the SN-DRG-DR preparation, afferent neural transmission was evoked from the SN by electrical stimulation and recorded at the split L6 DR. Seven naïve and six TNBS-treated C57BL/6 mice (8–16 weeks, 25–35 g, either sex) were used for the colorectum-PN-DRG-DR preparation and fourteen naïve C57BL/6 mice (8–16 weeks, 25–35 g, either sex) were used for the SN-DRG-DR preparation. Experimenters were not blinded to intracolonic treatment, but this

should not have significant impact on the objective single-fiber and GCaMP6f recordings from afferents.

*Ex vivo preparation of colorectum-PN-DRG-DR and SN-DRG-DR*. The same procedures described above in the single-fiber recordings section were used to perform mouse anesthesia, euthanasia and dorsal pediculectomy. As shown in **Figures 2A** and **2B**, the colorectum-PN-DRG-DR were carefully dissected and placed in the custom-built tissue chamber, which was circulated with oxygenated Krebs solution at 30°C. The L6 dorsal root was gently pulled into the adjacent recording chamber filled with mineral oil and split into fine filaments (~10 μm) for single-fiber recordings from individual afferent axons using a custom-built micro-wire electrode array reported previously [10]. As illustrated in **Figure 2C**, the colorectum was cannulated and connected to a custom-built CRD device consisting of four hydrostatic columns of phosphate buffered saline (PBS) set at 15, 30, 45 and 60 mmHg pressures, respectively. Computer-controlled solenoid valves were implemented to regulate the onset and termination of CRD, which reliably evoked neural response in colorectal afferents. In another series of experiments to monitor the effect of DRG stimulation, we evoked action potentials by electrical stimulation of the spinal nerve once every 2 sec and delivered synchronized trains of DRG stimulation between SN stimulations. Since electrical stimulation by-passed the nerve endings in the colorectum, we only harvested the SN-DRG-DR as displayed in **Figure 3A**.

*Protocol for DRG stimulation and CRD using the colorectum-PN-DRG-DR preparation*. The same needle electrode for characterizing the strength-duration curves described previously was used to deliver constant current stimulation to the caudal region of the L6 DRG, where the somata of high-threshold colorectal afferents are clustered [25]. Biphasic constant current stimuli (charge-balanced bipolar) generated by an IZ2H stimulator (Tucker-Davis Technologies Inc.,

Alachua, FL) were delivered to the L6 DRG at a wide frequency range from 10 to 1000 Hz. Stimulus pulse width was set to be either 0.1 or 0.2 msec based on the chronaxie measurement shown in **Figure 1C**. The amplitude of DRG stimulation was set to be suprathreshold so as to evoke action potentials in single-fiber recordings. In some experiments, subthreshold DRG stimulation was also tested during which no action potentials were evoked. As illustrated in **Figure 2D**, the CRD protocol was performed prior to (control), immediately after, and 15–30 min after DRG stimulation (recovery). A typical DRG stimulation protocol consisted of 30 pulse trains at 0.5 Hz train frequency and 0.5 sec inter-train intervals (60 sec in total). Pulse frequencies for DRG stimulation were set to be one of the following: 10, 50, 100, 500 or 1000 Hz. The CRD protocol consisted of four ascending pressure steps of 5 and 10 sec duration for TNBS-treated and naïve mice respectively and 8 sec inter-step intervals (15, 30, 45 and 60 mmHg).

*Protocol for synchronized SN and DRG stimulation with the SN-DRG-DR preparation.* The SN-DRG-DR were harvested in continuity as illustrated in **Figure 3A**. Neural transmission from the SN to the DR was evoked by electrical stimulation of the SN via a suction electrode pulled from a quartz glass capillary (tip Φ ~300 μm), which delivered cathodic constant current stimulation (0.2 msec pulse width, 0.2–2 mA pulse amplitude) via a stimulus isolator (A365, World Precision Instruments, New Haven, CT). To determine the threshold amplitude of DRG stimulation, we first evoked action potentials in the DR by stimulation of the SN or DRG at 0.5 Hz, a low frequency that will not cause marked activity-dependent slowing in unmyelinated C-fibers [46]. Stimulating the SN and DRG at 0.5 Hz can evoke activity in the same afferent as evidenced by identical waveforms in the single-fiber recording, but different conduction delays as shown in **Figure 3A**. Then, the threshold amplitude of DRG stimulation was determined by stimulating three locations along the axial length of the DRG to determine the minimal current

amplitude to evoke 3–5 action potentials with every 10 stimulus pluses (0.5 Hz). We set that DRG stimulation location for that afferent throughout an experiment. The DRG stimulus intensities were set to be either subthreshold or suprathreshold, corresponding to 70–80% and 120–150% of the threshold current amplitude, respectively.

To assess the effect of DRG stimulation on afferent neural transmission, we designed the temporally synchronized SN and DRG stimulation protocol as illustrated in **Figures 3B** and **3C**. The train frequencies of DRG stimulation and pulse frequency of SN stimulation were both set to be 0.5 Hz. The inter-train interval of DRG stimulation was set to be 0.5 sec, in the middle of which SN stimulation was delivered. The synchronized SN and DRG stimulation protocol consisted of 180 sec of combined SN and DRG stimulation, which was flanked by two 20-sec periods of stimulation of the SN alone before (control) and immediately after DRG stimulation. An additional 20-sec of SN stimulation was conducted 15–30 min after terminating DRG stimulation (recovery). In each DRG stimulation protocol, pulse frequency was set to be one of the following: 10, 50, 100, 500 or 1000 Hz.

*Data processing.* As described previously, action potentials evoked by either CRD or SN stimulation were recorded from split DR and processed off-line to identify individual action potentials and compute conduction velocity using customized MATLAB programs. The number of action potentials evoked by each CRD protocol was normalized to the number of action potentials evoked by 60 mmHg distension (=100%) in the control trial. Data were presented as means ± SE. One-way and Two-way ANOVA and Nonparametric Mann-Whitney Rank Sum or Kruskal Wallis comparisons were performed as appropriate using SigmaPlot v9.0. Differences were considered significant when $p < 0.05$.

**Effect of DRG stimulation in suppressing *in vivo* visceromotor responses (VMR) to colorectal distension**

*Surgical preparation for VMR recording and L6 DRG stimulation. In vivo* experiments were conducted on C57BL/6 mice (8–12 weeks of age, 25–35 g, either sex), which were euthanized right afterwards. First, mouse received one intraperitoneal injection of urethane (1.2 mg/kg), which preserved the spinal-bulbo-spinal reflex necessary for the behavioral VMR in rodents [5]. Then, surgical procedures were performed with mouse receiving additional 0.5–1% isoflurane anesthesia. A small incision (~10 mm) was made at the abdominal skin of a mouse in supine position to reveal both left and right oblique musculatures. For each of the two oblique muscles, two EMG wire electrodes (Teflon-coated stainless-steel wire, Cooner Wire, Chatworth, CA) were sutured on (Vicryl suture, Ethicon) and separated by ~1 mm for measuring the EMG responses to CRD. The abdominal incision was then closed by sutures and the mouse was flipped to a prone position. The dorsal side of the L6 vertebral segment was carefully exposed by dissecting away the muscle layers as displayed in **Figure 4A**. L6 pedicles and the lateral sides of laminae were then removed by trimming the bony structure using a fine-tipped (Φ ~20 μm) dental bur to expose both left and right L6 DRGs leaving the spinal canal and articular process intact as shown in **Figure 4A**. Special care was taken to avoid perforating the DRG capsule. The isoflurane anesthesia was reduced to 0–0.5% after completing the surgical procedures.

*Setup and protocol for DRG stimulation and colorectal distension in vivo.* A custom-built DRG stimulation electrode was made with platinum-iridium wire (Φ 250 μm, Pt80/Ir20, Goodfellow, UK) and placed in close proximity to L6 DRG for delivering electrical stimuli. To mitigate the movement artefact from respiration and motor reflex, the DRG stimulating electrode was fixed to a ring-shaped adaptor which was glued to the surrounding tissues as shown in **Figure**

**4B**. A magnified view of the exposed L6 DRG and the stimulating electrode is shown in **Figure 4C**. The L6 DRGs were covered with Krebs solution to keep the exposed DRG moist and provide electrical conduction for the stimulating electrode. A stimulus isolator (Model 4100, A-M Systems, Sequim, WA) was used to deliver biphasic constant current stimuli (charge-balanced bipolar) to the L6 DRG at either 10, 50 or 100 Hz. Stimulus pulse width was set to be either 0.1 or 0.2 msec based on the chronaxie measurement shown in **Figure 1C**. The amplitude of DRG stimulation was set to be 120% of the motor threshold i.e., stimulus threshold at which muscle twitch in limbs or lumbar segment was observed. In some experiments, subthreshold DRG stimulation (60% of the motor threshold) was also tested.

A lubricated polyethylene balloon (1 cm long, 0.6 cm diameter) was inserted into the colorectum and the connecting tube was taped to the tail. The rear end of the balloon was 5–10 mm deep inside the colorectum from the anal verge. The balloon was connected to the same custom-built distension device for single-fiber recordings as described above. EMG responses were recorded by a differential amplifier (Model 1700, A-M Systems, Sequim, WA) and a digitizer (CED 1401, Cambridge Electronic Design Limited, Cambridge, England). The schematic setup for recording the EMG responses to CRD and conducting L6 DRG stimulation is shown in **Figure 4D**. The protocol of conducting CRD and DRG stimulation was similar to in the aforementioned *ex vivo* single-fiber experiment. Baseline EMG activity was recorded for 10 sec prior to CRD which serves as a reference for EMG activity during CRD. The CRD protocol consisted of four ascending pressure steps (15, 30, 45 and 60 mmHg, all at 5 sec duration) separated by 8 sec between steps. To assess the effect of L6 DRG stimulation, VMR responses to CRD were recorded prior to, immediately after and 15–30 min after DRG stimulation.

*Data processing.* EMG activities evoked by CRD were recorded from the abdominal oblique musculature, digitized at 2000 Hz, and processed off-line using customized MATLAB programs. The EMG signals were rectified for calculating the area under the curve (AUC), which was used to evaluate the level of VMR to CRD [12]. VMR evoked by CRD was quantified as the AUC values during the 5-sec CRD subtracted by a 5-sec baseline AUC before the distension. The AUC values from four distending pressures (15–60 mmHg) were normalized by the AUC value from 60 mmHg CRD (100%) in the control trial (i.e., without DRG stimulation). Data were presented as means ± SE. One-way and Two-way ANOVA and nonparametric Kruskal Wallis comparisons were performed as appropriate using SigmaStat v4.0. Differences were considered significant when $p < 0.05$.

## Results

### Determination of chronaxie.

As summarized in **Figure 1C**, stimulus strength-duration curves were measured in 36 DRG neurons from 10 mice by single-fiber recordings from the split DR, of which 26 were Aδ-type with CV between 1 and 7.5 m/s and 10 were C-type with CV less than 1 m/s. The chronaxies were determined to be 105.7 ± 4.0 μsec for Aδ-type DRG neurons and 148.9 ± 11.1 μsec for C-type. Using GCaMP6f optical recording, 7 naïve and 8 TNBS-treated GCaMP6f transgenic mice were used to determine the chronaxie. For the naïve GCaMP6f mice, the strength-duration curves of 10 medium-diameter DRG neurons (20 μm < Φ < 35 μm) and 12 small-diameter DRG neurons (Φ < 20 μm) were quantified, the chronaxies of which were 75.0 ± 5.5 μsec and 153.4 ± 11.7 μsec, respectively. For the TNBS treated mice, 20 medium-diameter DRG neurons showed an average

chronaxie of 125.0 ± 9.9 μsec, and 16 small-diameter DRG neurons yielded an average chronaxie of 215.4 ± 13.7 μsec.

In naïve C57BL/6 or GCaMP6f transgenic mice, the chronaxies of C-type DRG neurons (by single-fiber recordings) and small-diameter DRG neurons (by optical recordings) were not statistically different (t-test, $p = 0.78$). The chronaxie values measured from Aδ-type fibers and medium-diameter DRG neurons differ slightly, but significantly (t-test, $p < 0.001$). The chronaxies were significantly different between Aδ-type and C-type DRG neurons as well as between medium- and small-diameter neurons (t-test, $p < 0.001$). TNBS treatment significantly increased the chronaxies for both medium- (t-test, $p < 0.05$) and small-diameter neurons (t-test, $p < 0.05$) as compared to in naïve GCaMP6f mice. To accommodate the stimulation of Aδ-type and C-type DRG neurons, we set the stimulus pulse width at 0.1 or 0.2 msec throughout the study.

**Suprathreshold DRG stimulation effectively blocks distension-evoked (i.e., mechanical) afferent neural transmission from the colorectum to the spinal cord.**

Using the colorectum-PN-DRG-DR preparation, afferent action potentials were evoked by graded CRD and recorded as single-units from split DR in both naïve and TNBS treated mice as shown in **Figures 5A** and **5B**, respectively. A detailed view of CRD-evoked colorectal afferent activities is displayed in **Figure 5C**. The neural transmission in colorectal afferents was blocked or attenuated immediately after suprathreshold DRG stimulation at all five tested pulse frequencies (10, 50, 100, 500 and 1000 Hz). In contrast, sub-threshold DRG stimulation of 50 and 100 Hz did not block colorectal afferent transmission in either naïve or TNBS-treated mice, frequencies at which complete conduction block was achieved at suprathreshold stimulation.

Suprathreshold DRG stimulation was assessed in 9 colorectal afferents from 7 naïve mice and 9 afferents from 6 TNBS-treated mice as summarized in **Figure 6**, where the number of evoked

spikes was normalized to the number of spikes evoked by the 60 mmHg pressure step in control trials prior to DRG stimulation. Immediately after DRG stimulation, responses to CRD were significantly reduced at all five tested frequencies of DRG stimulation (10, 50, 100, 500 and 1000 Hz) for both naïve and TNBS-treated mice as shown in **Figures 6A** and **6B**, respectively (Two-way ANOVA, Bonferroni post-hoc comparison, $p < 0.001$ for control vs. after in naïve and TNBS treated mice). Responses to CRD recovered completely 15–30 min after terminating DRG stimulation (post-hoc comparison for control vs. recovery, $p > 0.5$ in naïve mice and $p > 0.25$ in TNBS-treated mice for all five frequencies). CRD responses at 60 mmHg pressure were normalized and were plotted in insets for **Figures 6A** and **6B** after DRG stimulation at all five frequencies (10, 50, 100, 500 and 1000 Hz) for naïve and TNBS-treated mice, respectively. DRG stimulation by all five frequencies significantly attenuated afferent responses as compared to control (One-way ANOVA, $p < 0.05$ for control vs. 10, 50, 100, 500 and 1000 Hz in both naïve and TNBS-treated mice). The inhibitory effect of 50 Hz DRG stimulation was significantly greater than 10, 500 or 1000 Hz in naïve mice (One-way ANOVA, $p < 0.025$ for 50 vs. 10, 500 and 1000 Hz). In TNBS-treated mice, the inhibitory effect of 50 Hz stimulation was significantly greater than 10 or 1000 Hz (One-way ANOVA, $p < 0.047$ for 50 vs. 10 and 1000 Hz). Similarly, 100 Hz stimulation showed significantly greater inhibitory effect than 10 or 1000 Hz in both naïve and TNBS treated mice (One-way ANOVA, $p < 0.05$ for 100 vs. 10 or 1000 Hz). There was no statistical difference between 50 and 100 Hz or between 100 and 500 Hz stimulations in either naïve or TNBS groups ($p = 0.527$ for 50 vs. 100 Hz, $p = 0.063$ for 100 vs. 500 Hz in naïve mice; $p = 0.305$ for 50 vs. 100 Hz, $p = 0.096$ for 100 vs. 500 Hz in TNBS treated mice). Comparing the naïve and TNBS groups, there was no significant difference in the inhibitory effect of DRG stimulation to suppress the transmission of spikes evoked by 60 mmHg distension (One-way

ANOVA, $p > 0.17$). Also, the recovered responses to 60 mmHg CRD at 15–30 min after DRG stimulation were not significantly different between naïve and TNBS groups (One-way ANOVA, $p > 0.29$).

**Suprathreshold DRG stimulation progressively increased afferent conduction delay and led to conduction block.**

The neuromodulatory effect of DRG stimulation as assessed immediately after the DRG stimulation is shown in **Figures 7** and **8**. Our mechanical CRD stimuli presented significant technical challenges to study the instantaneous effect of DRG stimulation on afferent transmission during the course of CRD. We addressed the challenge by using a SN-DRG-DR preparation as described in the Methods, which allowed instantaneous monitoring of afferent transmission during DRG stimulation. As shown by single-fiber recordings from typical Aδ- and C-fibers in **Figure 7A**, action potentials were evoked by SN stimulation and recorded at L6 DR. The conduction delay (CD) of individual afferents was assessed prior to (as control), during, and after DRG stimulation once every 2 sec. SN stimulation was applied once every 2 sec, each one of the SN stimulation was assigned with a stimulation index number. The CD of a typical Aδ- and a C-fiber were plotted against the SN stimulation index and displayed in **Figure 7B**. The CD increased instantaneously and progressively during suprathreshold DRG stimulation and both afferents in **Figure 7** eventually failed to conduct action potentials following suprathreshold DRG stimulation. Afferent transmission was fully recovered 15–30 min after terminating suprathreshold DRG stimulation. We also assessed the effect of subthreshold DRG stimulation (70–80% of the threshold current amplitude) on afferent neural transmission using the same synchronized SN and DRG stimulation protocol. As shown in **Figure 7B**, 50 and 100 Hz subthreshold DRG stimulation, frequencies that demonstrated optimal blocking efficiency by suprathreshold stimulation (see insets in **Figures 6A**

and **B),** did not affect conduction delay or block afferent transmission even after 15 min of DRG stimulation.

The neuromodulatory effects of suprathreshold DRG stimulation were studied in 31 Aδ-type afferents (N = 29 for 10 Hz; N = 30 for 1000 Hz; N = 31 for 50, 100, and 500 Hz) and 22 C-type afferents at five stimulus frequencies (10, 50, 100, 500, 1000 Hz) from 14 mice, the results of which were summarized in **Figure 8**. The blocking effects of suprathreshold DRG stimulation (10–1000 Hz) on a typical Aδ- and a C-fibers are displayed in **Figure 8A**. A complete afferent transmission block was defined as the continuous absence of action potentials in the recording for at least 20 sec (10 SN stimulations). As summarized in **Figure 8B**, complete transmission block is frequency dependent. DRG stimulation at 50, 100 and 500 Hz blocked 87%, 90%, and 74% of the tested Aδ-fibers, respectively. In comparison, 10 and 1000 Hz stimulation only blocked 27% and 36% of Aδ-fibers. Similarly, C-fibers were preferentially blocked by 50 and 100 Hz DRG stimulation (86% and 77%) rather than by lower (10 Hz at 68%) or higher (500 Hz at 54%, 1000 Hz at 45%) frequencies. DRG stimulation at 10 Hz blocked a significantly greater proportion of C-fibers than Aδ-fibers (Fisher's exact test, $p = 0.005$). Frequencies above 10 Hz showed no statistical difference in blocking Aδ- and C-fibers (Fisher's exact test, $p = 1$, 0.253, 0.155 and 0.576 for 50, 100, 500 and 1000 Hz, respectively).

In afferents with complete transmission block, the cumulative positive electrical charge delivered to the DRG before a complete block was calculated by integrating the positive part of the stimulus pulses (charge balanced) from the onset of DRG stimulation to the onset of transmission block. The total charge to block is summarized in **Figure 8C**, which shows a monotonous increase with increased stimulus frequency. The required charge to block Aδ-fibers was significantly greater than required to block C-fibers only at 1000 Hz stimulation (Two-way

ANOVA, Aδ- vs. C-fibers, $p = 0.005$; post-hoc comparison, $p = 0.004$ for 1000 Hz and $p > 0.9$ for other frequencies).

Typically, the increase in conduction delay peaked right before the complete afferent block (see **Figure 8A** for 100 Hz stimulation). The maximum increase in CD for each afferent was measured in both blocked and unblocked afferents and was summarized in **Figure 8D**. Some afferents were blocked after the first 1.5-sec-long pulse train of DRG stimulation, and their CD increase could not be quantified and so were arbitrarily assigned to be the upper boundary (120%) and marked with stars in **Figure 8D**. The average maximum CD increase was 39.1 ± 4.4% in blocked Aδ-fibers, significantly higher than in unblocked Aδ-fibers (25.6 ± 4.9%, One-way ANOVA, $p = 0.046$). Similarly, the average maximum CD increase was significantly higher in blocked C-fibers (51.9 ± 5.9%) than in unblocked C-fibers (27.9 ± 4.4%, $p = 0.003$). Between Aδ- and C-fibers, there were not statistical differences in maximum CD increase within either blocked or unblocked groups (One-way ANOVA, $p = 0.094$ and 0.765 for blocked and unblocked groups, respectively).

The histogram of baseline conduction velocity from 31 Aδ-fibers and 22 C-fibers subjected to DRG stimulation is displayed in **Figure 9A** and the scatter plot of those afferents at different CV undergoing DRG stimulation at all five tested frequencies is shown in **Figure 9B.** The blocking effect of DRG stimulation appears dependent on both the stimulus frequency and the CV of the individual afferent. Stimulus frequencies of 50 and 100 Hz efficiently blocked greater than 85% of tested afferents across the entire range of CVs (0.3 to 7 m/s). There is no statistical difference in CV between the blocked and unblocked afferents at 50 and 100 Hz (Mann-Whitney Rank Sum Test, $p = 0.503$ and 0.115 at 50 and 100 Hz, respectively). Lower and higher stimulus frequencies were not efficient in blocking afferents at certain CV as shown in **Figure 9A** and **9B**. At 10 Hz

DRG stimulation, only slower conducting afferents were blocked, none of the afferents with CV faster than 3 m/s were blocked. The average CV of blocked afferents by 10 Hz stimulation is significantly slower than the unblocked counterpart (Mann-Whitney Rank Sum Test, $p < 0.001$). Similarly, 500 Hz stimulation preferentially blocked afferents with CV greater than 0.7 m/s, and the average CV of blocked afferents is faster than unblocked counterpart (Mann-Whitney Rank Sum Test, $p = 0.007$). For 1000 Hz DRG stimulation, there is no statistical difference in average CV between blocked and unblocked afferents (Mann-Whitney Rank Sum Test, $p = 0.654$).

**Suprathreshold L6 DRG stimulation (10–100 Hz) significantly attenuates *in vivo* visceromotor responses to colorectal distension.**

In urethane-anesthetized mice, the VMR to CRD as a metric of noxious visceral stimulus was quantified by EMG activities recorded from abdominal oblique musculature as shown in **Figure 10A**. The EMG activities during CRD were attenuated immediately after the suprathreshold DRG stimulation at 10, 50 and 100 Hz. The EMG responses recovered 15–30 minutes after terminating the DRG stimulation. In contrast, sub-threshold DRG stimulation had no apparent effect on VMR to CRD as shown in the grey traces in **Figure 10A**. Displayed in **Figure 10B** is summarized results of *in vivo* DRG stimulation from 7 mice. The AUC of rectified EMG signals were subtracted by the baselined AUC before the distension and normalized to the AUC of EMG signal from 60 mmHg distension in control trials prior to DRG stimulation. The AUC values of EMG responses evoked by CRD were significantly reduced immediately after DRG stimulation at all three tested frequencies (Two-way ANOVA, Bonferroni post-hoc comparison, $p < 0.001$ for control vs. after at 10, 50 and 100 Hz). The AUC of EMG responses recovered completely 15–30 min after DRG stimulation (post-hoc comparison for control vs. recovery, $p = 1$ for all three frequencies). The AUC values of EMG response to 60 mmHg pressure CRD were

normalized and plotted in **Figure 10C** after 10, 50 and 100 Hz DRG stimulation, which revealed significant inhibition of VMR to CRD by DRG stimulation (One-way ANOVA, $p < 0.001$ for control vs. 10, 50 and 100 Hz, respectively). The inhibitory effects of 50 and 100 Hz DRG stimulation were significantly greater than 10 Hz (One-way ANOVA, $p < 0.001$ for 100 vs. 10 Hz, $p = 0.004$ for 50 vs 10 Hz). The inhibitory effect between 50 and 100 Hz was not significantly different (One-way ANOVA, $p = 0.628$).

## Discussion

Reversible peripheral nerve block by electrical stimulation holds great clinical potential and has been thoroughly reviewed [41]. Anodal nerve block with direct current stimulation leads to imbalanced electro-chemical reactions at the electrode-tissue interface and is reserved as a research tool to selectively block myelinated axons [42]. Charge-balanced kilohertz stimulation (usually 1 to 30 kHz) reversibly blocks peripheral nerves with rapid onset, modest carry-over effects, and no apparent tissue damage, which has demonstrated efficacy in clinical applications [41]. In contrast, the relatively few reports on nerve block using sub-kilohertz stimulation are found either to implement charge-unbalanced stimulation [47] or to cause no conduction block, but depletion of neural transmitters [13]. By using *in vivo* single-fiber recordings, a most recent report did show that 20 Hz DRG stimulation effectively blocks neural transmission in rodent somatic afferents [6]. Consistent with that study, our current report shows that visceral afferents can also be blocked by sub-kilohertz charge-balanced stimulation at the DRG. We also provide functional evidence confirming attenuation of reflex response to noxious visceral stimulation, and thus support DRG stimulation as a possible therapeutic approach to visceral pain.

We document that DRG stimulation at 50 Hz efficiently blocks neural transmission in greater than 85% of thinly myelinated Aδ- and unmyelinated C-type afferents, which can be potentially applied for managing pain from pelvic visceral organs predominantly innervated by C-fibers and Aδ-fibers, including the urinary bladder, uterus, prostate, colon and rectum. We set the DRG stimulus amplitude slightly (20–50%) above the threshold, an intensity unlikely to cause permanent neural damage. In support, the conduction of both electrically and mechanically evoked action potentials recovers completely within 15–30 min after terminating DRG stimulation. It is worth mentioning that almost all prior reports quantify the effect of neuromodulation by either compound action potentials (CAP) or physiological functions of attached organs (e.g., bladder pressure or muscle forces) [41; 57]. CAPs as temporal and spatial summations of neural activities from bulk nerve bundles are not sensitive enough to detect neuromodulatory effects on individual axons [28]. In particular, slow-conducting C- and Aδ-fibers are under-represented in the amplitudes of CAPs compared to Aα- and Aβ-fibers [16], rendering CAPs unsuitable for studying slow-conducting visceral afferents. Physiological functions allow convenient assessment of efferent nerve block [13; 57], but cannot be applied to studying sensory afferents. In this study, we conduct single-fiber recordings at dorsal roots to record action potentials transmitted from peripheral axons, which provides direct evidence of reversible conduction block by DRG stimulation. Although a powerful method, single-fiber recordings have been utilized only by a few studies to assess neuromodulatory effects [6; 28], due to the challenges of recording single-units from peripheral axons [10]. Recent advances in microelectrode arrays interfacing with peripheral nerves [26] will likely allow a broader application of single-fiber recordings in neuromodulation research.

We determine strength-duration curves from intact DRG through single-fiber recordings and GCaMP6f recordings to establish an appropriate stimulus pulse width near the chronaxie to achieve better energy efficiency of neural stimulation [22]. Single-fiber recordings from attached dorsal roots allow classification of afferents into C- and Aδ-types based on conduction velocity. Using GCaMP6f recordings, we measure strength-duration curves in small- (< 20 μm) and medium- (20 to 35 μm) diameter DRG neurons and class them as C- and Aδ-type afferents because rodent DRG soma size correlates with axon myelination [35; 54]. Chronaxies determined using both methods are comparable and not statistically different. The short chronaxies (75–215 μsec) indicate that spike initiation by DRG stimulation is unlikely to be in the somata, but at attached axons, because chronaxies of neural somata are usually longer than 1 msec [43; 48]. Indeed, chronaxies are longer than 2 msec for dissociated human DRG neurons [45] and shorter than 665 μsec for human sensory nerves [37]. It is noteworthy that the above reported chronaxies were measured from dissociated DRG neurons, which may have altered ion channel composition and density from neurons in intact DRG. In the central nervous system, chronaxies are much shorter in axons (30–700 μsec) than in somata (1–10 msec) [43; 48]. Also, we observe in GCaMP6f recordings that it is usually not the neurons next to the stimulus electrode, but those further from the electrode are evoked by threshold DRG stimulation. Collectively, the results indicate that DRG stimulation outside the dura mater likely activates the attached axons for spike initiation, rather than the neural somata. The exact region of spike initiation requires further focused studies on the stem region and t-junction of the afferent neurons by using voltage-sensitive or sodium-sensitive dyes.

We speculate that the conduction block produced by DRG stimulation occurs at the t-junction based on two categories of evidence. First, spike transmission from the peripheral to the

central axons (i.e., through-conduction) does not require bifurcating propagation into the soma, and changes in soma conductance have minimal effects on the through-conduction [2]. Hence, blocking the stem region or soma likely has no appreciable effects on the through-conduction. Second, the safety factor for spike through-conduction is the lowest at the t-junction, as supported by substantial experimental evidence [14; 15; 23; 34; 50]. Computational simulations further confirm that propagation failure likely occurs at bifurcating points like the t-junction [2; 51; 58]. We report that supra-threshold, not sub-threshold DRG stimulation blocks afferent conduction, which suggests an activity-dependent mechanism of conduction block at the t-junction. Extensive studies have been conducted to reveal a low-pass "filtering" function of the t-junction that causes conduction failure at higher spiking frequencies [1; 23; 34]. Repetitive spiking can cause depolarization in some DRG somata and hyperpolarization in others [1; 23; 34]. Neither soma hyperpolarization nor depolarization seems to have direct influence on through-conduction at the t-junction [23]. Studies focusing on $Ca^{2+}$ concentrations indicate that the "filtering" function of the t-junction is calcium-dependent [23; 24; 33]. Thus, membrane hyperpolarization likely occurs at the t-junction via $Ca^{2+}$-mediated ion channels, e.g., $Ca^{2+}$-activated $K^+$ channels [23]. Also, an increase in $Na^+$ concentration is apparent even after a few action potentials in the confined axonal space [21], which can hyperpolarize the t-junction membrane by reducing the $Na^+$ reversal potential. In addition, persistent soma hyperpolarization can electrotonically hyperpolarize the t-junction membrane of those afferents with short and large-diameter stem axons as reported by a theoretical study [51]. In support, pharmacological hyperpolarization of soma membrane potential enhances afferent conduction failure and reduces rodent behavioral responses to noxious paw stimuli [14]. Synchronized DRG and nerve stimulation in the present study reveals a monotonous activity-dependent slowing of conduction velocities following DRG stimulation, which also lends

support to hyperpolarization at the t-junction for conduction block. Notably, Aδ- and C-fibers blocked by DRG stimulation show significantly greater increases in conduction delay than their unblocked counterparts (see **Figure 8D)**. Collectively, evidences presented here implicate membrane hyperpolarization as a plausible mechanism for activity-dependent conduction block at the t-junction. The exact molecular mechanisms require further studies.

We observe that mid-range DRG stimulation frequencies (50 to 500 Hz) are more efficient in blocking conduction than the lower (10 Hz) or higher (1 kHz) frequencies tested. Prior research indicates pronounced activity-dependent slowing in conduction velocities in nociceptive C-fibers when stimulus frequency is greater than 2 Hz [46]. As shown in **Figure 9**, 10 Hz DRG stimulation selectively blocks C-fibers and some slower-conducting Aδ-fibers, whereas none of the Aδ-fibers with CVs greater than 3 m/s are blocked. This is likely due to the prominent activity-dependent slowing in C-fibers [46]. In contrast, Aδ-fibers with CVs greater than 3 m/s show limited activity-dependent slowing at 10 Hz DRG stimulation (data not shown), which agrees with previous observations that activity-dependent slowing is not prominent in fast-conducting A-fibers [49; 52]. At 100 and 500 Hz stimulation, we note progressive increases in conduction delay (i.e., slowing) in Aδ-fibers, which likely accounts for the block effects in those fibers. For C-fibers, DRG stimulation beyond 50 Hz results in a gradual reduction in blocking probability. This is likely because C-fibers fire at less than 20 Hz physiologically and cannot follow higher stimulation frequency [11; 32]. Similarly, blocking probability is reduced for Aδ-fibers with further increases in stimulus frequency beyond 500 Hz. Stimulation in the kilohertz range generally does not reliably evoke action potentials and is considered sub-threshold stimulation [4]. The blocking effect of 50 to 100 Hz DRG stimulation was further validated by *in vivo* recordings of visceromotor responses to colorectal distension, a pseudoeffective reflex response widely used in the literature to quantify

the level of noxious visceral stimulation in rodents [38], thereby objectifying the experience of visceral pain. The *in vivo* outcome that 50 and 100 Hz DRG stimulation has significantly greater inhibition on VMR response than 10 Hz stimulation well agrees with the findings from *ex vivo* single-fiber recordings. We were unable to assess the *in vivo* effect of 500 and 1000 Hz DRG stimulation as suprathreshold stimulation at those high frequencies evoked tetanic contraction of limb muscles to confound the VMR responses.

In summary, we report that L6 DRG stimulation effectively blocks distension-evoked (i.e. mechanical) afferent neural transmission from the colorectum to the spinal cord in the sub-kilohertz range (10–1000 Hz); 50 and 100 Hz stimulation produce superior blocking probability than stimulation at 10, 500 or 1000 Hz. Using synchronized DRG and L6 spinal nerve stimulation, we find that DRG stimulation causes activity-dependent conduction slowing in both C- and Aδ-type afferents. Afferents blocked by DRG stimulation exhibit a significantly greater increase in conduction delay than unblocked counterparts. Mid-range stimulation frequencies block conduction more efficiently and produce greater activity-dependent slowing than either low (10 Hz) or high (1000 Hz) frequency stimulation. We report the average chronaxie of L6 DRG stimulation to be below 216 μsec for C-fibers and 125 μsec for Aδ-fibers, which indicates spike initiation likely at the attached afferent axons rather than in somata. The monotonous and progressive increase in conduction delay during DRG stimulation supports hyperpolarization of the t-junction as the underlying mechanism of conduction block. The blocking effect of 50 and 100 Hz DRG stimulation is further validated by an *in vivo* experiment showing suppressed visceromotor responses to colorectal distension in urethane-anesthetized mice. The results reported here draw attention to a new mechanism of afferent modulation that sub-kilohertz DRG

stimulation is capable of blocking conduction in C- and Aδ-fibers, a promising neuromodulation strategy for managing chronic visceral pain.

**Acknowledgments**

We sincerely thank Dr. G. F. Gebhart for editing the manuscript and providing constructive feedbacks. This work was supported by NSF CAREER 1844762 and NIH R01 DK120824 grants awarded to Dr. Bin Feng. There is no conflict of interest to declare.

REFERENCES

[1] Amir R, Devor M. Spike-evoked suppression and burst patterning in dorsal root ganglion neurons of the rat. The Journal of physiology 1997;501 ( Pt 1)(Pt 1):183-196.

[2] Amir R, Devor M. Electrical excitability of the soma of sensory neurons is required for spike invasion of the soma, but not for through-conduction. Biophys J 2003;84(4):2181-2191.

[3] Baranidharan G, Simpson KH, Dhandapani K. Spinal cord stimulation for visceral pain--a novel approach. Neuromodulation 2014;17(8):753-758; discussion 758.

[4] Chakravarthy K, Richter H, Christo PJ, Williams K, Guan Y. Spinal Cord Stimulation for Treating Chronic Pain: Reviewing Preclinical and Clinical Data on Paresthesia-Free High-Frequency Therapy. Neuromodulation 2018;21(1):10-18.

[5] Chang HH, Yeh JC, Mao J, Ginsberg DA, Ghoniem G, Rodriguez LV. Spinal cord stimulation ameliorates detrusor over-activity and visceromotor pain responses in rats with cystitis. Neurourol Urodyn 2019;38(1):116-122.

[6] Chao D, Zhang Z, Mecca CM, Hogan QH, Pan B. Analgesic dorsal root ganglionic field stimulation blocks conduction of afferent impulse trains selectively in nociceptive sensory afferents. Pain 2020;161(12):2872-2886.

[7] Chen L, Guo T, Siri S, Feng B. Frequency-dependent modulation of action potential transmission in afferent axons by DRG stimulation. Neuroscience 2019, Society for Neuroscience. Chicago, IL, 2019.

[8] Chen L, Guo T, Siri S, Feng B. Suprathreshold DRG stimulation blocks action potential transmission in afferent axons while subthreshold stimulation does not. Biomedical Engineering Society 2019 Annual Fall Meeting. Philadelphia, PA, 2019.

[9] Chen L, Ilham SJ, Feng B. Pharmacological Approach for Managing Pain in Irritable Bowel Syndrome: A Review Article. Anesth Pain Med 2017;7(2):e42747.

[10] Chen L, Ilham SJ, Guo T, Emadi S, Feng B. In vitro multichannel single-unit recordings of action potentials from mouse sciatic nerve. Biomed Phys Eng Express 2017;3.

[11] Chen X, Levine JD. Altered temporal pattern of mechanically evoked C-fiber activity in a model of diabetic neuropathy in the rat. Neuroscience 2003;121(4):1007-1015.

[12] Christianson JA, Gebhart GF. Assessment of colon sensitivity by luminal distension in mice. Nat Protoc 2007;2(10):2624-2631.

[13] Dowden BR, Wark HA, Normann RA. Muscle-selective block using intrafascicular high-frequency alternating current. Muscle Nerve 2010;42(3):339-347.

[14] Du X, Hao H, Gigout S, Huang D, Yang Y, Li L, Wang C, Sundt D, Jaffe DB, Zhang H, Gamper N. Control of somatic membrane potential in nociceptive neurons and its implications for peripheral nociceptive transmission. Pain 2014;155(11):2306-2322.

[15] Fang X, McMullan S, Lawson SN, Djouhri L. Electrophysiological differences between nociceptive and non-nociceptive dorsal root ganglion neurones in the rat in vivo. J Physiol 2005;565(Pt 3):927-943.

[16] Feng B, Chen L, Ilham SJ. A Review on Ultrasonic Neuromodulation of the Peripheral Nervous System: Enhanced or Suppressed Activities? Applied Sciences 2019;9(8):1637.

[17] Feng B, Guo T. Visceral pain from colon and rectum: the mechanotransduction and biomechanics. Journal of Neural Transmission 2020;127(4):415-429.

[18] Feng B, La JH, Schwartz ES, Gebhart GF. Irritable bowel syndrome: methods, mechanisms, and pathophysiology. Neural and neuro-immune mechanisms of visceral

hypersensitivity in irritable bowel syndrome. Am J Physiol Gastrointest Liver Physiol 2012;302(10):G1085-1098.

[19] Feng B, La JH, Schwartz ES, Tanaka T, McMurray TP, Gebhart GF. Long-term sensitization of mechanosensitive and -insensitive afferents in mice with persistent colorectal hypersensitivity. Am J Physiol Gastrointest Liver Physiol 2012;302(7):G676-683.

[20] Feng B, La JH, Tanaka T, Schwartz ES, McMurray TP, Gebhart GF. Altered colorectal afferent function associated with TNBS-induced visceral hypersensitivity in mice. Am J Physiol Gastrointest Liver Physiol 2012;303(7):G817-824.

[21] Feng B, Zhu Y, La JH, Wills ZP, Gebhart GF. Experimental and computational evidence for an essential role of NaV1.6 in spike initiation at stretch-sensitive colorectal afferent endings. J Neurophysiol 2015;113(7):2618-2634.

[22] Geddes LA, Bourland JD. The strength-duration curve. IEEE Trans Biomed Eng 1985;32(6):458-459.

[23] Gemes G, Koopmeiners A, Rigaud M, Lirk P, Sapunar D, Bangaru ML, Vilceanu D, Garrison SR, Ljubkovic M, Mueller SJ, Stucky CL, Hogan QH. Failure of action potential propagation in sensory neurons: mechanisms and loss of afferent filtering in C-type units after painful nerve injury. J Physiol 2013;591(4):1111-1131.

[24] Gemes G, Rigaud M, Koopmeiners AS, Poroli MJ, Zoga V, Hogan QH. Calcium signaling in intact dorsal root ganglia: new observations and the effect of injury. Anesthesiology 2010;113(1):134-146.

[25] Guo T, Bian Z, Trocki K, Chen L, Zheng G, Feng B. Optical recording reveals topological distribution of functionally classified colorectal afferent neurons in intact lumbosacral DRG. Physiol Rep 2019;7(9):e14097.

[26] Guo T, Chen L, Tran K, Ghelich P, Guo Y, Nolta N, Emadi S, Han M, Feng B. Extracellular single-unit recordings from peripheral nerve axons in vitro by a novel multichannel microelectrode array. Sensors and Actuators B: Chemical 2020;315:128111.

[27] Hayar A, Gu C, Al-Chaer ED. An improved method for patch clamp recording and calcium imaging of neurons in the intact dorsal root ganglion in rats. J Neurosci Methods 2008;173(1):74-82.

[28] Ilham SJ, Chen L, Guo T, Emadi S, Hoshino K, Feng B. In vitro single-unit recordings reveal increased peripheral nerve conduction velocity by focused pulsed ultrasound. Biomed Phys Eng Express 2018;4(4).

[29] Kapural L, Nagem H, Tlucek H, Sessler DI. Spinal cord stimulation for chronic visceral abdominal pain. Pain Med 2010;11(3):347-355.

[30] Khan YN, Raza SS, Khan EA. Application of spinal cord stimulation for the treatment of abdominal visceral pain syndromes: case reports. Neuromodulation 2005;8(1):14-27.

[31] Koopmeiners AS, Mueller S, Kramer J, Hogan QH. Effect of electrical field stimulation on dorsal root ganglion neuronal function. Neuromodulation 2013;16(4):304-311; discussion 310-301.

[32] Leem JW, Willis WD, Chung J. Cutaneous sensory receptors in the rat foot. Journal of neurophysiology 1993;69(5):1684-1699.

[33] Lüscher C, Lipp P, Lüscher HR, Niggli E. Control of action potential propagation by intracellular Ca2+ in cultured rat dorsal root ganglion cells. The Journal of physiology 1996;490 ( Pt 2)(Pt 2):319-324.

[34] Luscher C, Streit J, Lipp P, Luscher H. Action potential propagation through embryonic dorsal root ganglion cells in culture. II. Decrease of conduction reliability during repetitive stimulation. Journal of Neurophysiology 1994;72(2):634-643.

[35] Ma C, LaMotte RH. Multiple Sites for Generation of Ectopic Spontaneous Activity in Neurons of the Chronically Compressed Dorsal Root Ganglion. The Journal of Neuroscience 2007;27(51):14059-14068.

[36] Mekhail N, Deer TR, Kramer J, Poree L, Amirdelfan K, Grigsby E, Staats P, Burton AW, Burgher AH, Scowcroft J, Golovac S, Kapural L, Paicius R, Pope J, Samuel S, McRoberts WP, Schaufele M, Kent AR, Raza A, Levy RM. Paresthesia-Free Dorsal Root Ganglion Stimulation: An ACCURATE Study Sub-Analysis. Neuromodulation 2019.

[37] Mogyoros I, Kiernan MC, Burke D. Strength-duration properties of human peripheral nerve. Brain 1996;119(2):439-447.

[38] Ness TJ, Gebhart GF. Colorectal distension as a noxious visceral stimulus: physiologic and pharmacologic characterization of pseudaffective reflexes in the rat. Brain Res 1988;450(1-2):153-169.

[39] Pan B, Zhang Z, Chao D, Hogan QH. Dorsal Root Ganglion Field Stimulation Prevents Inflammation and Joint Damage in a Rat Model of Rheumatoid Arthritis. Neuromodulation 2018;21(3):247-253.

[40] Parker JL, Cameron T. Technology for Peripheral Nerve Stimulation. Prog Neurol Surg 2015;29:1-19.

[41] Patel YA, Butera RJ. Challenges associated with nerve conduction block using kilohertz electrical stimulation. Journal of Neural Engineering 2018;15(3):031002.

[42] Petruska JC, Hubscher CH, Johnson RD. Anodally focused polarization of peripheral nerve allows discrimination of myelinated and unmyelinated fiber input to brainstem nuclei. Experimental brain research 1998;121(4):379-390.

[43] Ranck JB, Jr. Which elements are excited in electrical stimulation of mammalian central nervous system: a review. Brain Res 1975;98(3):417-440.

[44] Ruscheweyh R, Forsthuber L, Schoffnegger D, Sandkuhler J. Modification of classical neurochemical markers in identified primary afferent neurons with Abeta-, Adelta-, and C-fibers after chronic constriction injury in mice. J Comp Neurol 2007;502(2):325-336.

[45] Scott BS, Petit TL, Becker LE, Edwards BAV. Electric membrane properties of human DRG neurons in cell culture and the effect of high K medium. Brain Research 1979;178(2):529-544.

[46] Serra J, Campero M, Ochoa J, Bostock H. Activity-dependent slowing of conduction differentiates functional subtypes of C fibres innervating human skin. The Journal of physiology 1999;515 ( Pt 3)(Pt 3):799-811.

[47] Solomonow M, Eldred E, Lyman J, Foster J. Fatigue considerations of muscle contractile force during high-frequency stimulation. Am J Phys Med 1983;62(3):117-122.

[48] Stern S, Agudelo-Toro A, Rotem A, Moses E, Neef A. Chronaxie Measurements in Patterned Neuronal Cultures from Rat Hippocampus. PloS one 2015;10(7):e0132577-e0132577.

[49] Stöhr M. Activity-dependent variations in threshold and conduction velocity of human sensory fibers. Journal of the Neurological Sciences 1981;49(1):47-54.

[50] Stoney SD. Limitations on impulse conduction at the branch point of afferent axons in frog dorsal root ganglion. Experimental Brain Research 1990;80(3):512-524.

[51] Sundt D, Gamper N, Jaffe DB. Spike propagation through the dorsal root ganglia in an unmyelinated sensory neuron: a modeling study. Journal of neurophysiology 2015;114(6):3140-3153.

[52] Thalhammer JG, Raymond SA, Popitz-bergez FA, Strichartz GR. Modality-Dependent Modulation of Conduction by Impulse Activity in Functionally Characterized Single Cutaneous Afferents in the Rat. Somatosensory & Motor Research 1994;11(3):243-257.

[53] Verrills P, Mitchell B, Vivian D, Cusack W, Kramer J. Dorsal Root Ganglion Stimulation Is Paresthesia-Independent: A Retrospective Study. Neuromodulation 2019.

[54] Wang J, La J-H, Hamill OP. PIEZO1 Is Selectively Expressed in Small Diameter Mouse DRG Neurons Distinct From Neurons Strongly Expressing TRPV1. Frontiers in Molecular Neuroscience 2019;12(178).

[55] Yu G, Segel I, Zhang Z, Hogan QH, Pan B. Dorsal Root Ganglion Stimulation Alleviates Pain-related Behaviors in Rats with Nerve Injury and Osteoarthritis. Anesthesiology 2020;133(2):408-425.

[56] Zhang TC, Janik JJ, Grill WM. Mechanisms and models of spinal cord stimulation for the treatment of neuropathic pain. Brain Res 2014;1569:19-31.

[57] Zhang Z, Lyon TD, Kadow BT, Shen B, Wang J, Lee A, Kang A, Roppolo JR, Groat WCd, Tai C. Conduction block of mammalian myelinated nerve by local cooling to 15–30°C after a brief heating. Journal of Neurophysiology 2016;115(3):1436-1445.

[58] Zhou L, Chiu SY. Computer model for action potential propagation through branch point in myelinated nerves. J Neurophysiol 2001;85(1):197-210.

**Figures and figure legends**

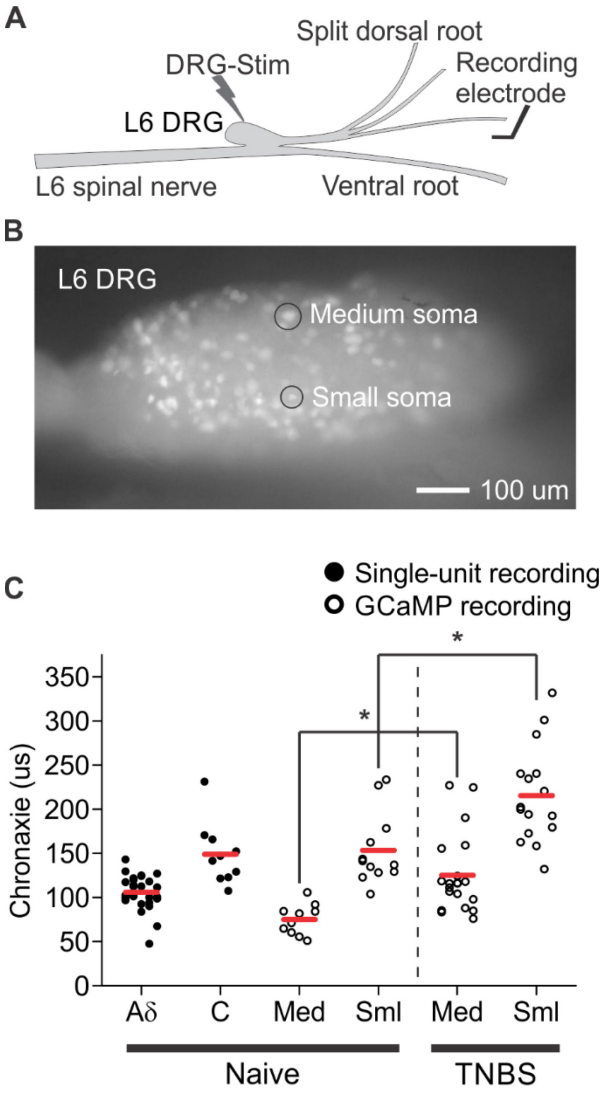


**Figure 1. Determination of the chronaxie of electrical DRG stimulation by single-fiber (A) and optical GCaMP6f recordings (B) in naïve and TNBS-treated mice.** (A) Schematic of L6 DRG stimulation and single-fiber recordings from a split L6 dorsal root. DRG neurons are classified as Aδ- or C-fiber based on conduction velocity (Aδ, 1 to 7.5 m/s; C, < 1 m/s). (B) GCaMP6f recordings of $Ca^{2+}$ transients at 60–100 frames/sec using a sCMOS camera. Identical DRG stimulation protocols are used as in single-fiber recordings. DRG somata are grouped as medium- or small-diameter neurons (20 to 35 µm, < 20 µm), which generally correlate with Aδ-

and C-fibers, respectively. (C) The summarized chronaxies of DRG stimulation determined by single-fiber recordings in naïve mice (solid dots) and GCaMP6f recordings in naïve and TNBS-treated mice (hollow dots). Asterisks indicate $p < 0.05$. Med: medium-diameter neuron; Sml: small-diameter neuron.

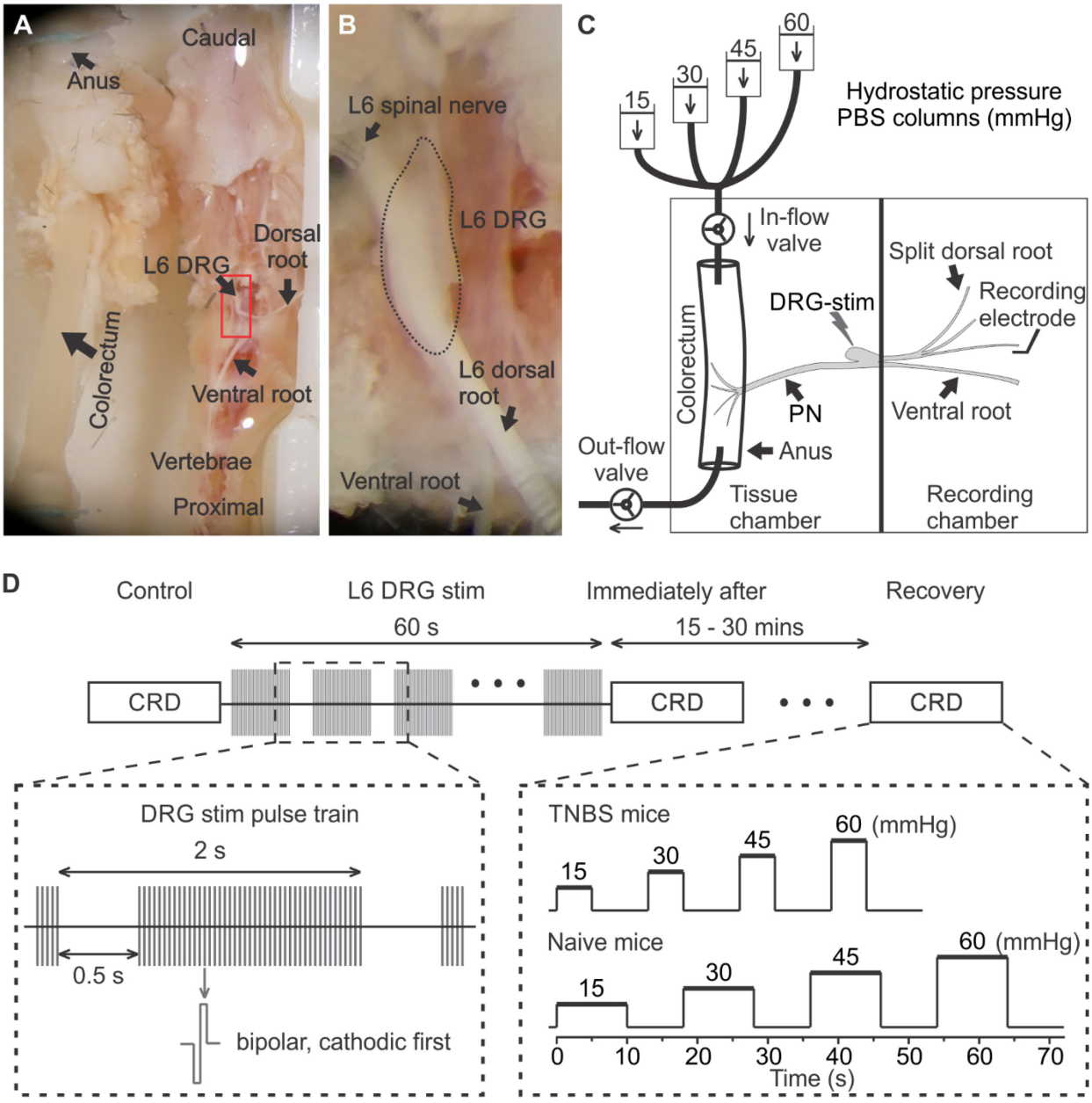

**Figure 2. Assessing the efficacy of DRG stimulation to block distension-evoked (mechanical) afferent transmission using colorectum-PN-DRG-DR preparation.** A photograph of the *ex vivo* preparation with colorectum, pelvic nerve, L6 spinal nerve, DRG, and dorsal root in continuity, i.e., the colorectum-PN-DRG-DR preparation is displayed in (A); a magnified view of the area inside the red box is displayed in (B). The outer boundary of the L6 DRG is marked by a dashed line. (C) Schematic of single-fiber recordings of afferent action potentials from split DR evoked by colorectal distension. DRG stimulation is delivered to the L6 DRG by a blunt-tipped needle electrode. (D) Schematic of the protocol to assess the efficacy of DRG stimulation on colorectal afferent neural transmission. Action potentials evoked by CRD are recorded prior to (control), immediately after, and 15–30 min after (recovery) DRG stimulation. The duration of pressure steps in the CRD protocol for TNBS-treated and naïve mice are 5 and 10 sec, respectively. The interval between successive pressure steps is 8 sec.

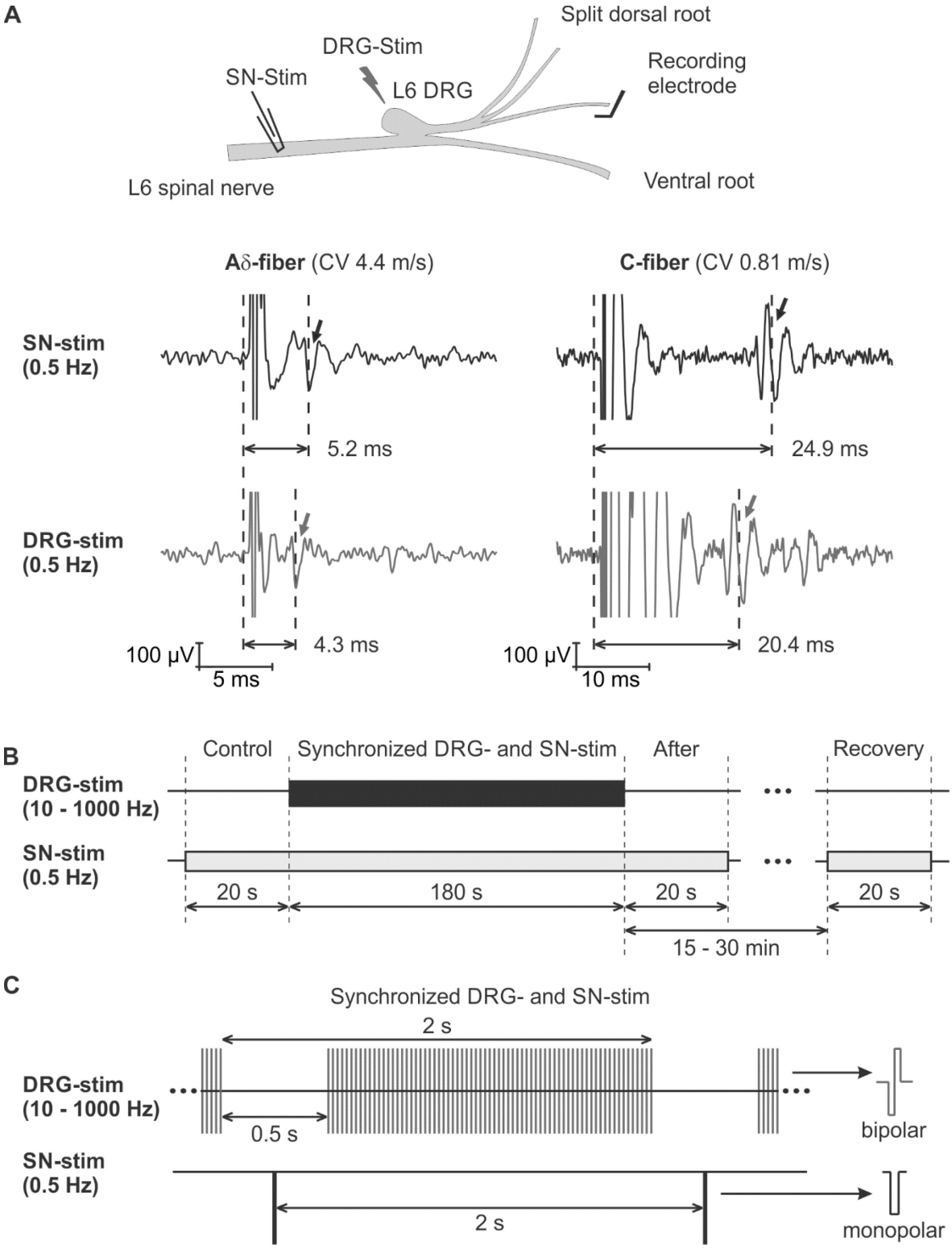


**Figure 3. Assessing the instantaneous effect of DRG stimulation on the transmission of electrically evoked action potentials from the spinal nerve.** (A) Schematic of the *ex vivo*

preparation with mouse L6 spinal nerve, DRG and dorsal root in continuity, i.e., the SN-DRG-DR preparation. Electrical stimulation of the SN or DRG at 0.5 Hz activates the same afferent in the single-fiber recording with identical spike wave forms, but different conduction delays. (B) Protocol to assess the instantaneous effect of DRG stimulation on action potential transmission. SN and DRG stimulations are synchronized to allow measuring the conduction delay once every 2 sec during DRG stimulation. (C) Schematic of synchronized DRG and SN stimulation. DRG-stim: DRG stimulation; SN-stim: spinal nerve stimulation.

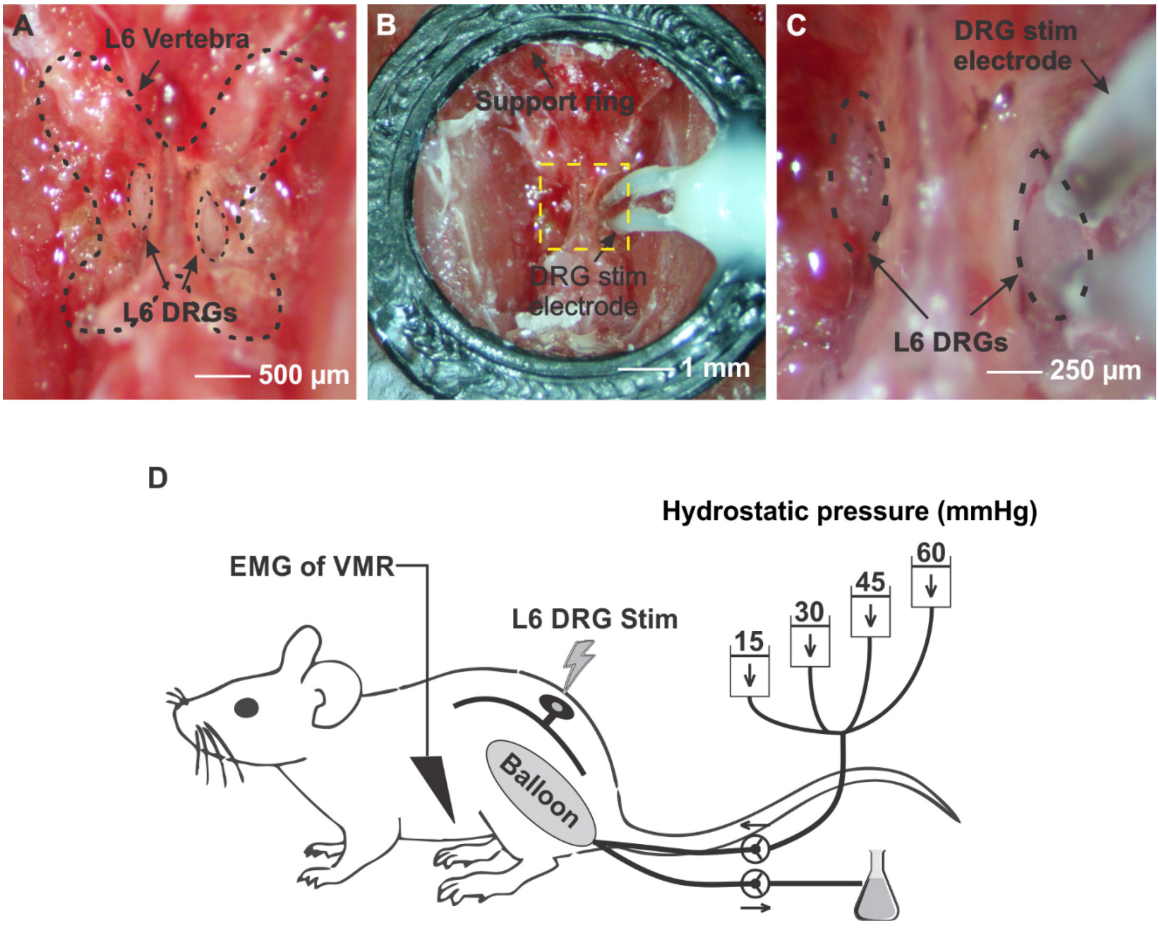


**Figure 4. *In vivo* L6 DRG stimulation to assess the effect of visceral motor responses to colorectal distension.** (A) A photograph of isolated L6 vertebra and exposed L6 DRG marked by black dashed line. (B) A 3D-printed adaptor ring with two wire electrodes attached is glued to the

surrounding tissue to ensure relative constant distance between the electrodes and DRG. (C) A magnified view of the area inside the yellow dashed box in (B). (D) The schematic for recording EMG signals from abdominal oblique musculature as a metric to evaluate VMR evoked by CRD.

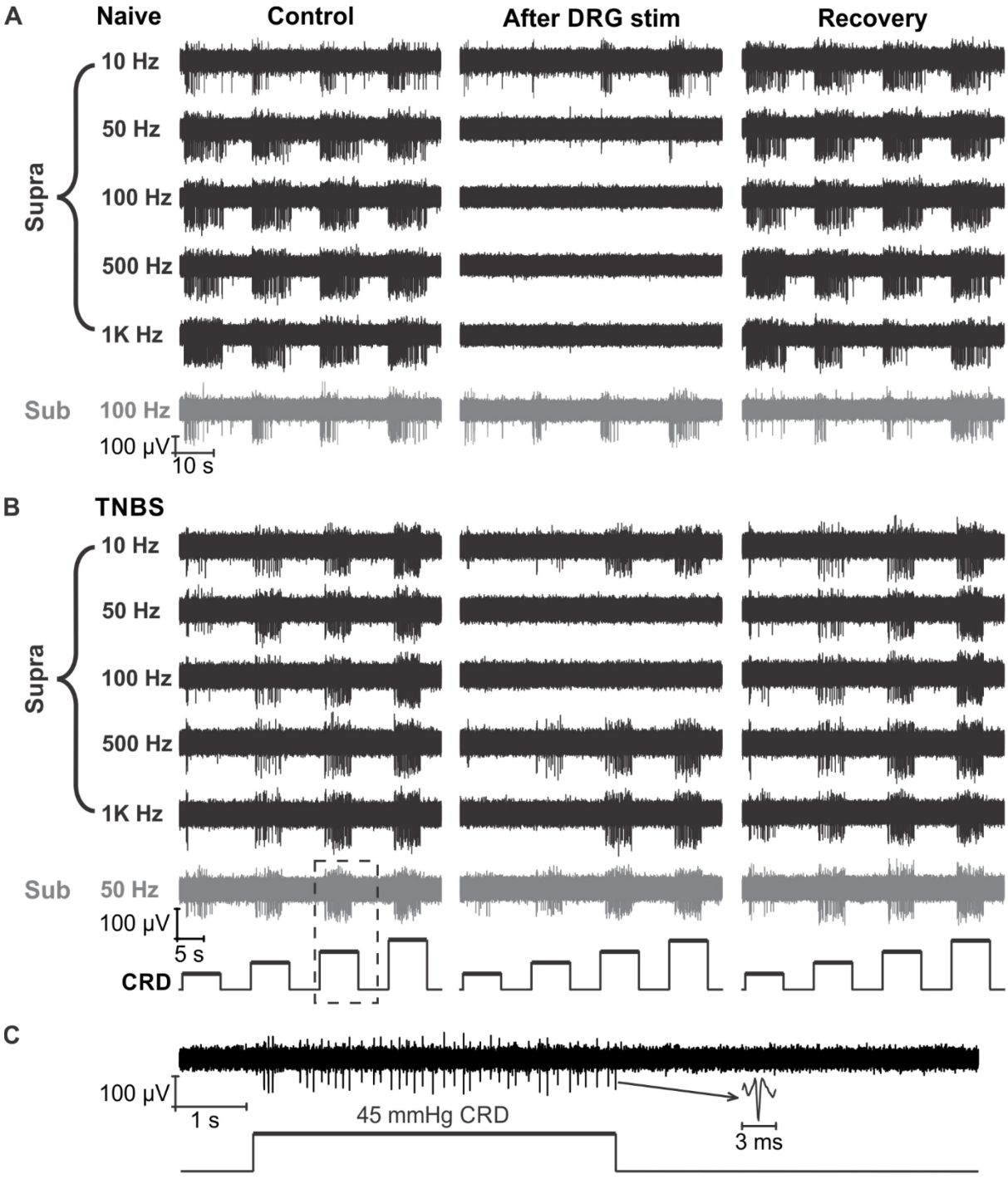

**Figure 5. Representative single-fiber recordings using the colorectum-PN-DRG-DR preparation showing inhibition of colorectal afferent transmission by suprathreshold DRG stimulation in both naïve (A) and TNBS-treated mice (B).** (A) Transmission of evoked action potentials by CRD is attenuated or completely blocked by suprathreshold DRG stimulation (235 μA, 0.1 msec duration) at all five tested frequencies (10, 50, 100, 500, 1000 Hz) and recovers within 15–30 min after terminating DRG stimulation. Subthreshold DRG stimulation (150 μA, 0.1 msec duration, 100 Hz) does not block afferent transmission of the same fiber, in contrast to the complete blocking effect by suprathreshold stimulation at 100 Hz. (B) Similar to (A), suprathreshold DRG stimulation (1 mA, 0.2 msec duration) suppresses transmission of evoked action potentials by CRD at all five tested frequencies, which recovers after terminating the DRG stimulation. Subthreshold DRG stimulation (700 μA, 0.2 msec duration, 50 Hz) does not block transmission in the same afferent fiber. (C) Magnified view of the dashed line box in (B) showing single-unit action potentials.

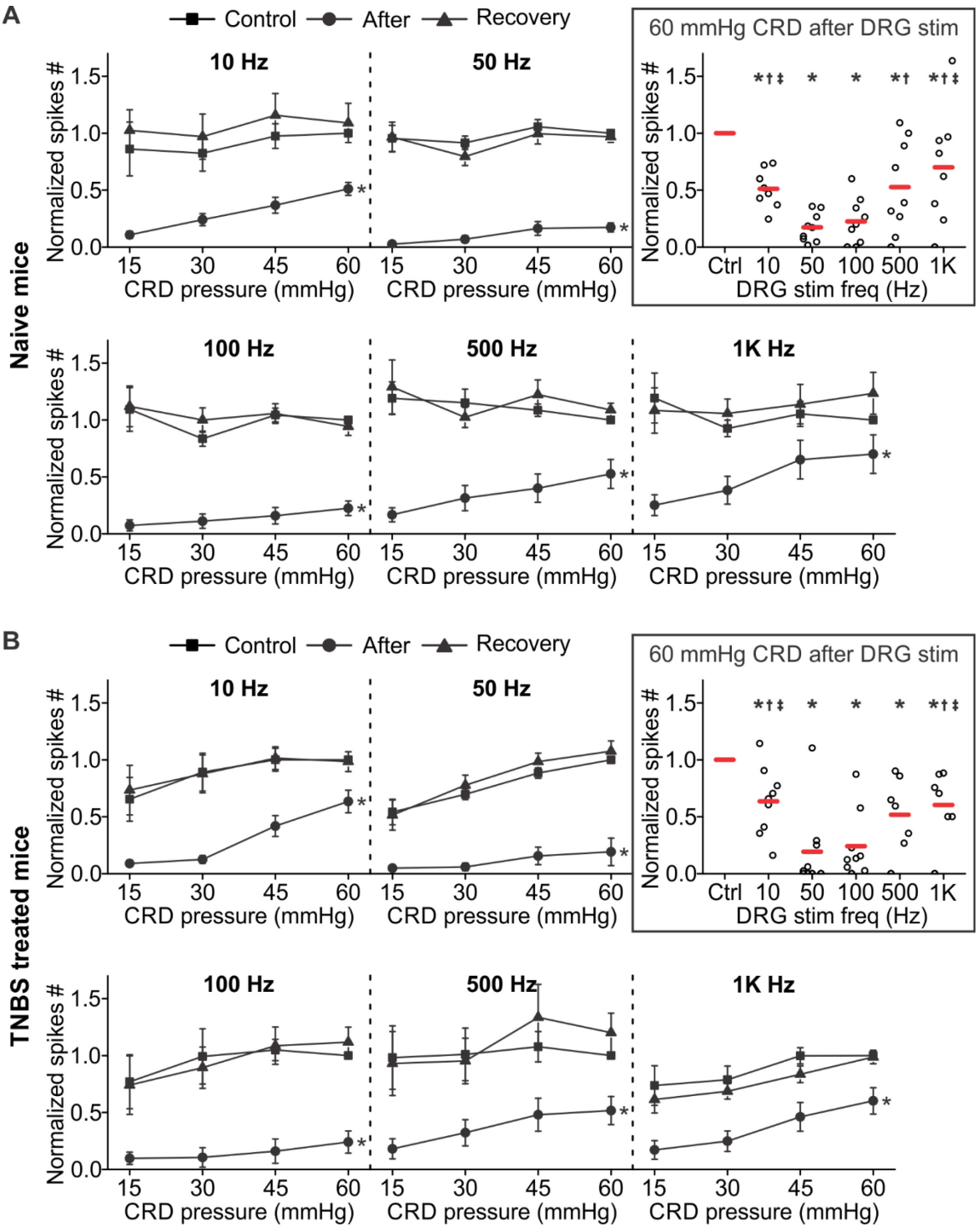


**Figure 6. Frequency-dependent inhibition of colorectal afferent transmission by suprathreshold DRG stimulation in both naïve and TNBS-treated mice.** DRG stimulation inhibits colorectal afferent transmission at all five tested frequencies: 10, 50, 100, 500 and 1000

Hz in naïve mice (A) and TNBS-treated mice (B). Responses to CRD prior to DRG stimulation serve as control; responses to CRD are also recorded immediately after (After) and 15–30 min after terminating DRG stimulation (Recovery). Normalized CRD responses to 60 mmHg pressure immediately after DRG stimulation across five tested frequencies are shown in insets in (A) and (B) for naïve and TNBS-treated mice, respectively. * indicates $p < 0.05$ compared with control, † indicates $p < 0.05$ compared with 50 Hz DRG stimulation. ‡ indicates $p < 0.05$ compared with 100 Hz DRG stimulation.

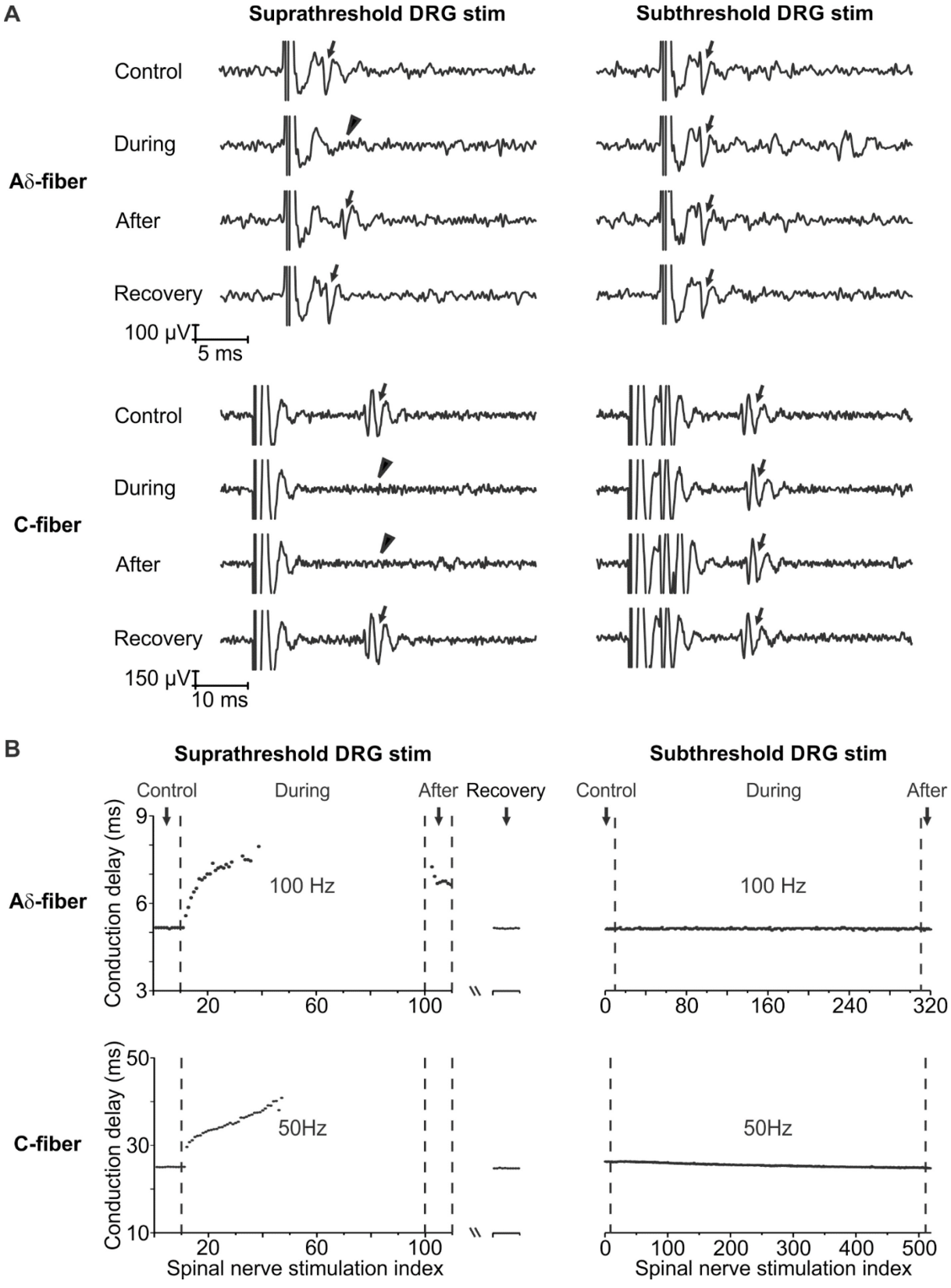
A
Suprathreshold DRG stim
Subthreshold DRG stim
Control
During
After
Recovery
Aδ-fiber
100 μV
5 ms
Control
During
After
Recovery
C-fiber
150 μV
10 ms
B
Suprathreshold DRG stim
Subthreshold DRG stim
Control
During
After
Recovery
Aδ-fiber
Conduction delay (ms)
100 Hz
C-fiber
50Hz
Spinal nerve stimulation index

**Figure 7. Representative single-fiber recordings in the SN-DRG-DR preparation showing instantaneous neuromodulation by suprathreshold DRG stimulation and no appreciable neuromodulation by subthreshold DRG stimulation.** (A) Typical single-fiber recordings from an Aδ- and a C-type afferent prior to, during, and after suprathreshold (left column) and subthreshold (right column) DRG stimulation. Recordings are also conducted 15–30 min after terminating DRG stimulation (recovery). Arrows: evoked action potential spikes; Arrow heads: absence of spikes. (B) The conduction delay of afferents in (A) are plotted against the SN stimulation index for both suprathreshold (left column) and subthreshold (right column) DRG stimulation.

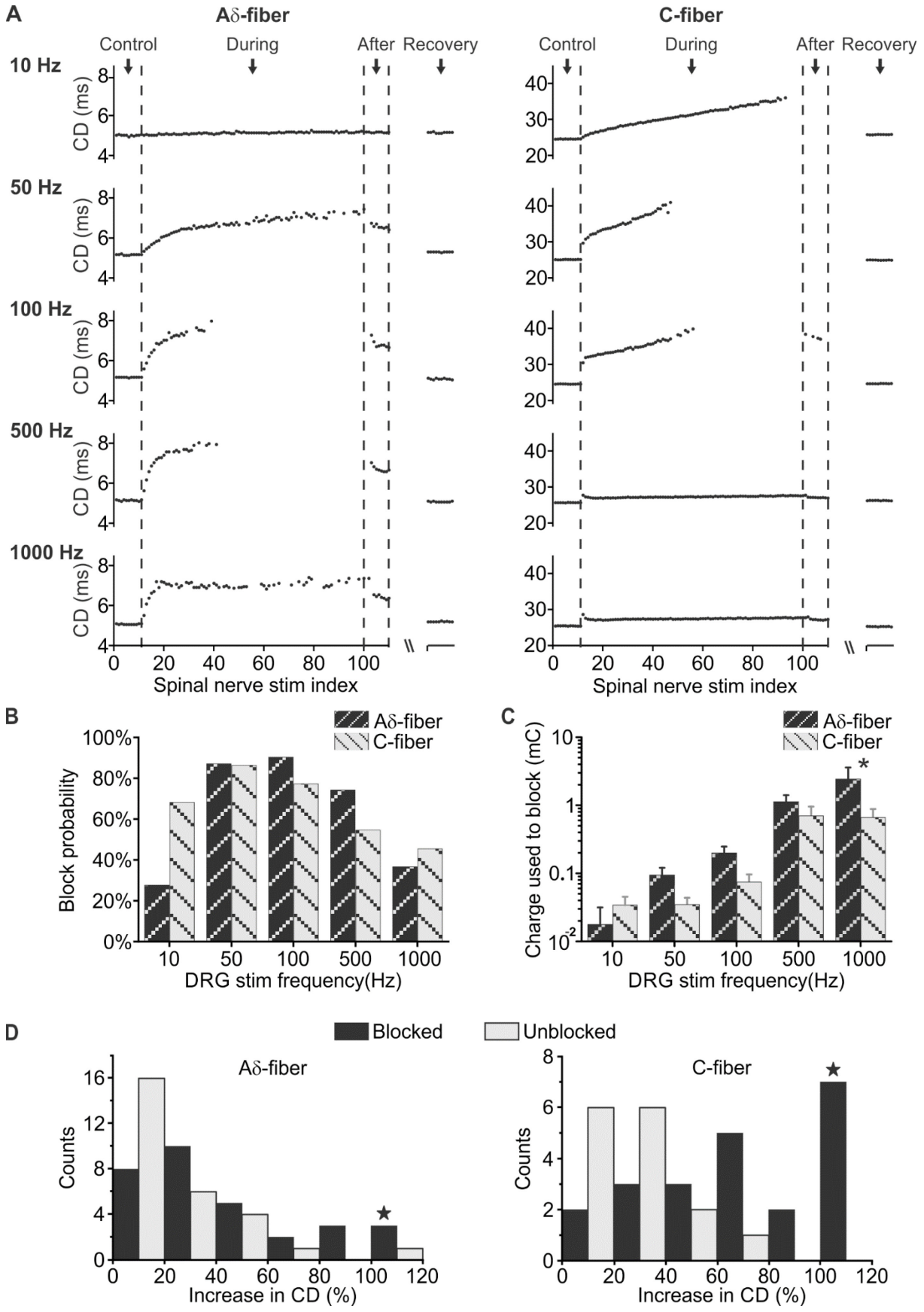
A
Aδ-fiber
C-fiber
Control
During
After
Recovery
10 Hz
50 Hz
100 Hz
500 Hz
1000 Hz
CD (ms)
Spinal nerve stim index
B
Aδ-fiber
C-fiber
Block probability
DRG stim frequency(Hz)
C
Charge used to block (mC)
DRG stim frequency(Hz)
D
Blocked
Unblocked
Counts
Increase in CD (%)

**Figure 8. Frequency-dependent conduction block of afferent neural transmission by suprathreshold DRG stimulation.** (A) Representative conduction delays recorded every 2 sec from representative Aδ- and C-fibers during DRG stimulation, 10–1000 Hz. (B) Summarized probability of complete transmission block by DRG stimulation, 10–1000 Hz. More than 74% of Aδ-type afferents are blocked by 50, 100 and 500 Hz stimulation, while the probability decreases to 36% at greater (1000 Hz) and to 27% at lower (10 Hz) frequencies. Over 77% of C-type afferents are blocked by 50 and 100 Hz DRG stimulation, and the probability decreases to 68% (10 Hz), 54% (500Hz) and 45% (1000 Hz). (C) Summarized total stimulus charge delivered to block action potential transmission. * indicates $p < 0.05$ when comparing Aδ- and C-fibers. (D) Histogram of maximum increase in conduction delay following DRG stimulation in Aδ- and C-fibers. Blocked fibers are labeled in black bars, unblocked fibers in gray bars. Some afferents are immediately blocked by the first 1.5-sec-long pulse train of DRG stimulation, and their CD increases are arbitrarily assigned to be 120%, i.e., bars marked with stars.

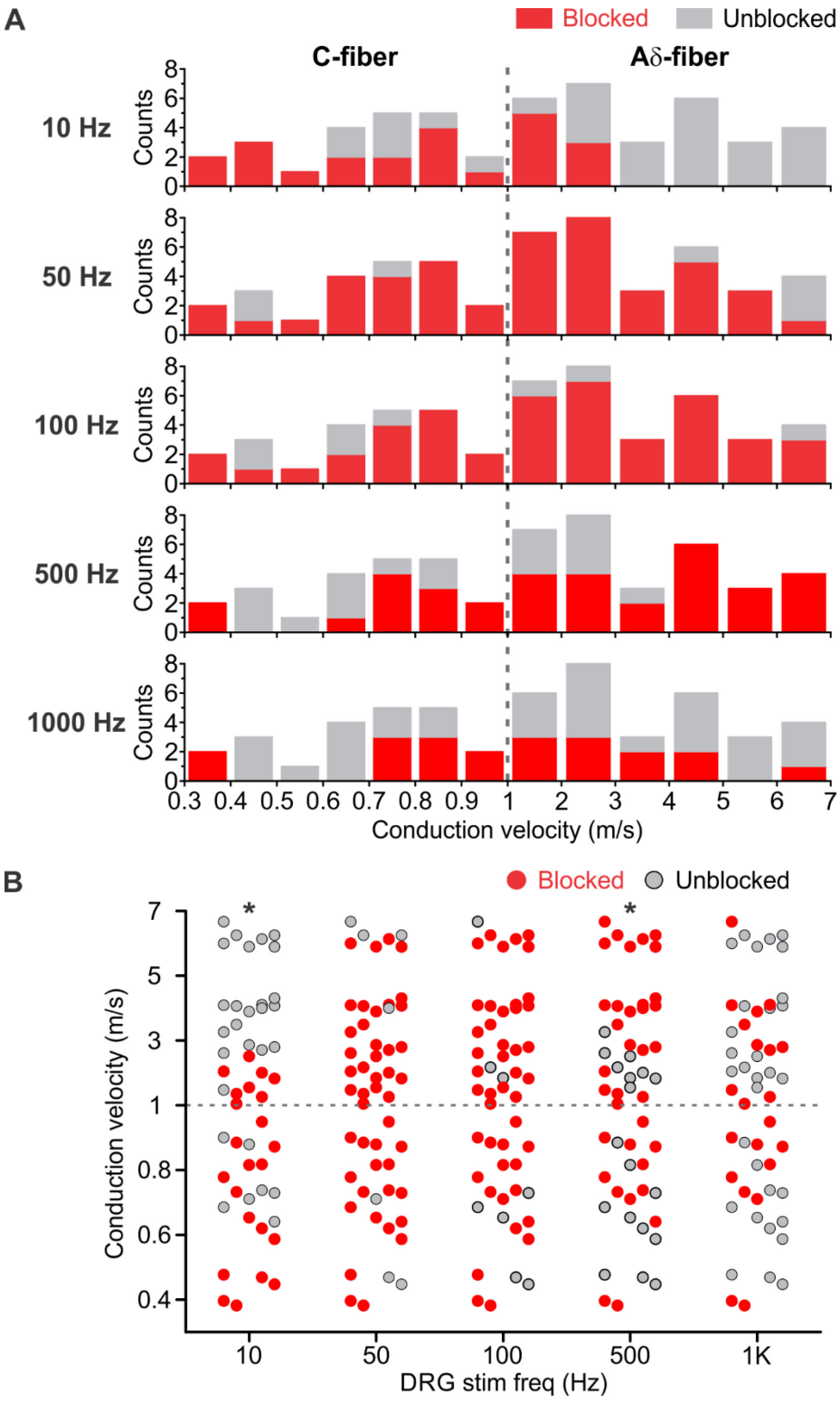


**Figure 9. Baseline conduction velocities (CV) of 31 Aδ-fibers and 22 C-fibers tested with DRG stimulation.** (A) Blocked afferents are represented by red bars and unblocked ones by gray

bars in the histogram of baseline CV. Mid-range frequencies of 50 and 100 Hz efficiently block afferents at all CVs (0.3–7 m/s). Afferents blocked by 10 Hz stimulation generally have CVs less than 3 m/s, whereas afferents blocked by 500 or 1000 Hz have CVs greater than 0.7 m/s. (B) Scatter plot of baseline CVs of afferents tested with DRG stimulation. Blocked afferents are represented by red dots and unblocked ones by gray dots. The average CVs of blocked and unblocked afferents are significantly different at 10 Hz DRG stimulation (Mann-Whitney Rank Sum Test, $p < 0.001$), so are at 500 Hz stimulation ($p = 0.007$). In contrast, CVs of blocked and unblocked afferents are not significantly different at 50, 100 or 1000 Hz DRG stimulation. Asterisks indicate $p < 0.05$ of CVs between blocked and unblocked afferents.

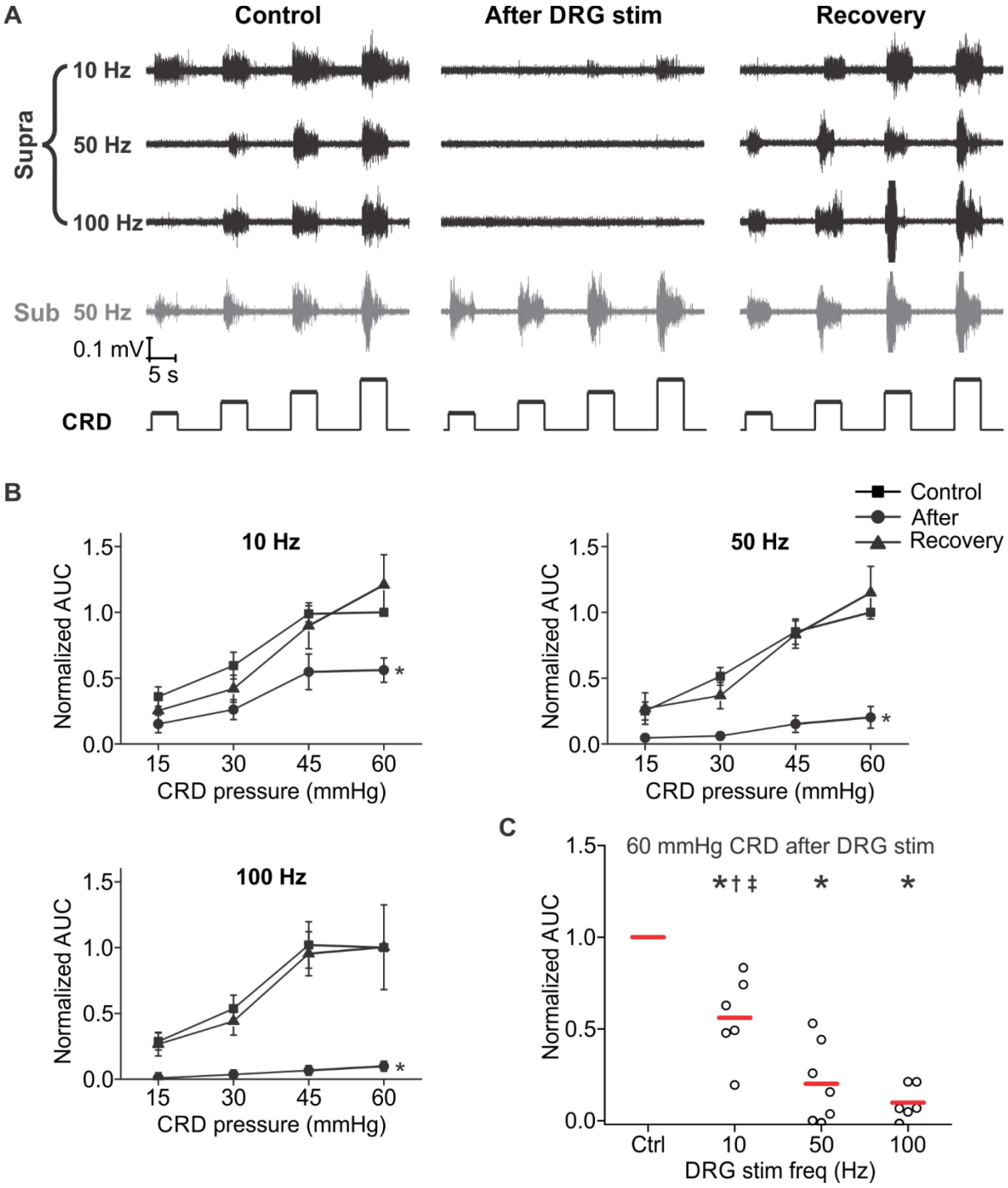


**Figure 10 Suprathreshold L6 DRG stimulation (10–100 Hz) significantly attenuates *in vivo* visceromotor responses evoked by colorectal distension.** (A) Representative EMG activities recorded at abdominal oblique musculature during the CRD protocol. EMG activities are

dramatically suppressed by suprathreshold L6 DRG stimulation (500 μA, 0.2 msec duration) at 10, 50 and 100 Hz. EMG responses recover to the control level 15–30 min after terminating the DRG stimulation. Subthreshold DRG stimulation (350 μA, 0.2 msec duration, 50 Hz) does not inhibit EMG activity. (B) Normalized area under the curve (AUC) values of EMG activity in response to CRD. EMG responses to CRD prior to DRG stimulation serve as control, which are also recorded immediately after (After) and 15–30 min after the termination of DRG stimulation (Recovery). (C) Normalized AUC values of EMG activities in response to 60 mmHg pressure distension immediately after DRG stimulation at 10, 50 and 100 Hz. * indicates $p < 0.05$ compared with control, † indicates $p < 0.05$ compared with 50 Hz DRG stimulation. ‡ indicates $p < 0.05$ compared with 100 Hz DRG stimulation.